



1 **The importance of alkyl nitrates and sea ice emissions to atmospheric** 2 **NO_x sources and cycling in the summertime Southern Ocean marine** 3 **boundary layer.**

4 Jessica M. Burger¹, Julie Granger², Emily Joyce³, Meredith G. Hastings³, Kurt A.M. Spence¹, Katy E.
5 Altieri¹

6 ¹Department of Oceanography, University of Cape Town, Rondebosch, 7701, South Africa

7 ²Department of Marine Sciences, University of Connecticut, Groton, 06340, USA

8 ³Department of Earth, Environmental and Planetary Sciences and Institute at Brown for Environment and Society, Brown
9 University, Providence, RI, 02906, USA.

10 *Correspondence to:* Jessica M. Burger (brgjes006@uct.ac.za)

11 **Abstract.** Atmospheric nitrate originates from the oxidation of nitrogen oxides (NO_x=NO+NO₂) and impacts both tropospheric
12 chemistry and climate. NO_x sources, cycling, and NO_x to nitrate formation pathways are poorly constrained in remote marine
13 regions, especially the Southern Ocean where pristine conditions serve as a useful proxy for the preindustrial atmosphere.
14 Here, we measured the isotopic composition ($\delta^{15}\text{N}$ and $\delta^{18}\text{O}$) of atmospheric nitrate in coarse-mode ($> 1\ \mu\text{m}$) aerosols collected
15 in the summertime marine boundary layer of the Atlantic Southern Ocean from 34.5°S to 70°S, and across the northern edge
16 of the Weddell Sea. The $\delta^{15}\text{N}\text{-NO}_3^-$ decreased with latitude from -2.7‰ to -43.1‰. The decline in $\delta^{15}\text{N}$ with latitude is
17 attributed to changes in the dominant NO_x sources: lightning at the low latitudes, oceanic alkyl nitrates at the mid latitudes,
18 and photolysis of nitrate in snow at the high latitudes. There is no evidence of any influence from anthropogenic NO_x sources
19 or equilibrium isotopic fractionation. Using air mass back trajectories and an isotope mixing model, we calculate that oceanic
20 alkyl nitrate emissions have a $\delta^{15}\text{N}$ signature of $-22.0\text{‰} \pm 7.5\text{‰}$. Given that measurements of alkyl nitrate contributions to
21 remote nitrogen budgets are scarce, this may be a useful tracer for detecting their contribution in other oceanic regions. The
22 $\delta^{18}\text{O}\text{-NO}_3^-$ was always less than 70‰, indicating that daytime processes involving OH are the dominant NO_x oxidation pathway
23 during summer. Unusually low $\delta^{18}\text{O}\text{-NO}_3^-$ values (less than 31‰) were observed at the western edge of the Weddell Sea. The
24 air mass history of these samples indicates extensive interaction with sea ice covered ocean, which is known to enhance peroxy
25 radical production. The observed low $\delta^{18}\text{O}\text{-NO}_3^-$ is therefore attributed to increased exchange of NO with peroxy radicals,
26 which have a low $\delta^{18}\text{O}$, relative to ozone, which has a high $\delta^{18}\text{O}$. This study reveals that the mid- and high-latitude surface
27 ocean may serve as a more important NO_x source than previously thought, and that the ice-covered surface ocean impacts the
28 reactive nitrogen budget as well as the oxidative capacity of the marine boundary layer.



29 **1 Introduction**

30 Atmospheric nitrate (NO_3^-), hereafter defined as gas phase nitric acid (HNO_3) and particulate NO_3^- (p- NO_3^-), impacts air quality
31 and climate by contributing to atmospheric particulate matter (Park & Kim, 2005), and influencing the Earth's radiative heat
32 budget (IPCC, 2013). It also plays a major role in the biogeochemical cycling of reactive nitrogen (Altieri et al., 2021). NO_3^-
33 aerosols originate from the oxidation of nitrogen oxides, collectively referred to as NO_x ($\text{NO}_x = \text{NO} + \text{NO}_2$). NO_x cycling
34 controls the chemical production of tropospheric ozone (O_3), a greenhouse gas and pollutant (Finlayson-Pitts & Pitts, 2000),
35 which in turn contributes to the oxidising capacity of the atmosphere (Alexander & Mickley, 2015). Globally, fossil fuel
36 combustion is the primary NO_x source (van der A, et al., 2008), which far exceeds natural emissions such as biomass burning
37 (Finlayson-Pitts & Pitts, 2000), soil processes (Davidson & Kinglerlee, 1997) and lightning (Schumann & Huntrieser, 2007).

38 Due to its remoteness, the summertime Southern Ocean marine boundary layer (MBL) can be representative of
39 preindustrial-like atmospheric conditions (Hamilton, et al., 2014). The chemical composition of the Southern Ocean MBL is
40 characterised by low NO_3^- concentrations (Virkkula, et al., 2006), representative of a background aerosol environment (i.e.,
41 minimal anthropogenic influence). Furthermore, the South Atlantic sector of the Southern Ocean is primarily influenced by
42 natural NO_x sources. During summer, high lightning activity over South America and southern Africa results in NO_x production
43 between approximately 40°S and the intertropical convergence zone (ITCZ) (Nesbitt, et al., 2000). As such, lightning is
44 expected to be the dominant NO_x source in the low latitude MBL (Schumann & Huntrieser, 2007; van der A, et al., 2008).
45 Because of its pristine nature, the summertime Southern Ocean serves as a unique region in which to study atmospheric
46 chemistry and is a useful preindustrial reference point for comparing the magnitude of anthropogenic aerosol impacts on
47 climate (Haywood & Boucher, 2000; Hamilton, et al., 2014).

48 The atmospheric chemistry of the polar MBL at the high southern latitudes differs from that of the mid- and low-latitude
49 MBL. During summer, high levels of photochemistry result in the emission of reactive gases from sea ice and snow cover in
50 the Antarctic. As a result, highly elevated concentrations of hydrogen oxide radicals ($\text{HO}_x = \text{OH} + \text{peroxy radicals}$), halogens,
51 nitrous acid (HONO), and NO_x have been observed during spring and summer in the polar regions (Brough et al., 2019).
52 Furthermore, photochemical production of NO_x within the surface snow of Antarctica and subsequent oxidation in the
53 overlying atmosphere represents a significant NO_3^- source to the Antarctic troposphere (Jones, et al., 2000; Jones, et al., 2001).
54 NO_3^- photolysis near the surface-air interface of ice crystals produces NO_2 (Grannas, et al., 2007; Jones, et al., 2000), which
55 can be released to the firn (i.e., the intermediate stage of ice between snow and glacial ice) air and escape the snowpack to the
56 overlying atmosphere (Erland, et al., 2013; Shi, et al., 2015; Shi, et al., 2018). During winter, additional NO_x sources to the
57 Antarctic atmosphere may include long-range transported peroxyacetyl nitrates (PAN) and stratospheric inputs (Savarino, et
58 al., 2007; Lee, et al., 2014; Walters, et al., 2019).

59 Emission of alkyl nitrates (a group of nitrogen gases collectively referred to as RONO_2) from the surface ocean have been
60 recently proposed as a potential NO_x source to the MBL in remote regions (Williams, et al., 2014; Fisher et al., 2018).
61 Observations of elevated MBL alkyl nitrate concentrations suggest that a direct oceanic source exists in both the tropics (Atlas,



62 et al., 1993; Blake, et al., 2003), and the high-latitude Southern Ocean (Blake, et al., 1999; Jones, et al., 1999). Although the
63 exact mechanism remains unclear, experimental evidence suggests that oceanic RONO₂ production occurs via photochemical
64 processes involving the aqueous phase reaction of RO₂, derived from the photolysis of oceanic dissolved organic matter and
65 NO, derived from seawater nitrite photolysis (Dahl, et al., 2003; Dahl & Saltzman, 2008). Supersaturated RONO₂ conditions
66 in the surface ultimately drive a net flux from the ocean to the atmosphere (Chuck, et al., 2002; Dahl, et al., 2005). The
67 photolysis of emitted RONO₂ and subsequent OH oxidation in the overlying atmosphere leads to NO_x formation (Fisher, et
68 al., 2018).

69 Current global atmospheric models suggest that oceanic RONO₂ represents a significant source of nitrogen (N) to the
70 Southern Ocean MBL, accounting for 20% to 60% of the reactive N pool at the high-latitudes (60°S to 90°S) (Fisher, et al.,
71 2018). However, only one small shipborne dataset with coincident ocean-atmosphere RONO₂ concentration measurements
72 exists to substantiate this notion (Hughes et al., 2008). Additionally, the NO_x source from RONO₂ degradation dominates
73 relative to model defined primary NO_x emission sources over the SO, which include shipping, aircraft and lightning (Fisher,
74 et al., 2018). However, the lack of seawater observations available to constrain Southern Ocean RONO₂ distributions hamper
75 the validation of model fluxes. Better understanding of the Southern Ocean RONO₂ source is required to improve simulations
76 and accurately evaluate its contribution to the Southern Ocean MBL NO_x budget.

77 1.1 Natural abundance isotopes of atmospheric nitrate

78 Measurements of the oxygen (O) and N stable isotope ratios of atmospheric NO₃⁻ can be used to constrain NO_x sources, NO-
79 NO₂ cycling, and NO_x to NO₃⁻ oxidation pathways, which are critical to our understanding of the reactive N budget in the
80 atmosphere. This technique has been applied in both polluted (Elliot, et al., 2007; Zong, et al., 2017), open ocean (Hastings,
81 et al., 2003; Morin, et al., 2009; Kamezaki, et al., 2019; Gobel, et al., 2013; Altieri, et al., 2013), and polar environments
82 (Morin et al., 2009; Walters et al., 2019). Stable isotope ratios are reported as a ratio of the heavy to light isotopologues of a
83 sample relative to the constant isotopic ratio of a reference standard, using delta (δ) notation in units of “per mil” (‰) following
84 Eq. (1):

$$85 \delta = \left(\frac{R_{sample}}{R_{standard}} - 1 \right) \times 1000 \quad (1)$$

86 where R represents the ratio of ¹⁵N/¹⁴N or ¹⁸O/¹⁶O in the sample and in the reference standard, respectively. The reference for
87 O is Vienna Standard Mean Ocean Water (VSMOW) and for N is atmospheric N₂ (Bolhke, et al., 2003).

88 When NO_x is converted to NO₃⁻, the N atom is conserved. As such, it is generally expected that the N stable isotope ratio
89 of atmospheric NO₃⁻ (δ¹⁵N-NO₃⁻) reflects the δ¹⁵N of the source NO_x, (Kendall, et al., 2007) plus any isotopic fractionation
90 associated with NO/NO₂ cycling or NO_x to NO₃⁻ conversion. For example, the δ¹⁵N of lightning generated NO_x is close to 0‰
91 (Hoering, 1957) and is distinct from stratospheric and snowpack NO_x. Savarino et al., (2007) used the degree of N₂O
92 destruction in the stratosphere and the associated isotopic fractionation to derive an Antarctic stratospheric δ¹⁵N-NO_x source
93 signature of 19‰ ± 3‰ (Savarino, et al., 2007). In contrast, snow emitted NO_x typically has a very low δ¹⁵N signature due to



94 the large fractionation ($^{15}\epsilon$) of $\sim -48\%$ (Berhanu et al., 2014 and 2015) associated with NO_3^- photolysis in the snowpack,
95 where $^{15}\epsilon$ of a reaction is the ratio of the rates with which the two isotopes of N are converted from reactant to product. If
96 equilibrium isotope fractionation during NO/NO_2 cycling occurs, it results in the ^{15}N enrichment of NO_2 such that the NO_3^-
97 formed from this NO_2 will have a higher $\delta^{15}\text{N}-\text{NO}_3^-$ than the initial NO_x source (Freyer, et al., 1993; Walters, et al., 2016).
98 Equilibrium isotope fractionation during the transformation of NO_x to NO_3^- also results in higher $\delta^{15}\text{N}-\text{NO}_3^-$ compared to the
99 original NO_x source (Walters & Michalski, 2015).

100 In contrast to N, the O stable isotope ratio of atmospheric NO_3^- ($\delta^{18}\text{O}-\text{NO}_3^-$) is reflective of the oxidants involved in NO_x
101 cycling prior to NO_3^- formation, as well as the dominant NO_3^- formation pathway (Hastings, et al., 2003; Michalski, et al.,
102 2003; Alexander, et al., 2020). The O atoms of NO_x are rapidly exchanged with oxidising agents in the atmosphere to produce
103 NO_3^- . Tropospheric NO_x recycles rapidly with O_3 following the equations below:



106 The oxidation of NO to NO_2 requires an atmospheric oxidant, typically O_3 throughout most of the troposphere (R1), while the
107 breakdown of NO_2 back to NO is photolytic and requires light (R2). Therefore, under nighttime/dark conditions (R2) shuts
108 down and NO_x is comprised almost entirely of NO_2 .

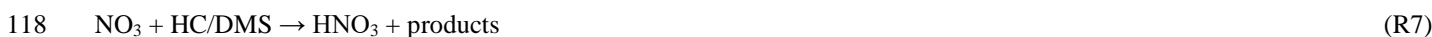
109 The dominant daytime sink for NO_x is the oxidation of NO_2 by OH , which produces nitric acid (HNO_3) via (R3), where M is
110 a non-reacting molecule.



112 Under nighttime/dark conditions, the photolytic production of OH cannot occur and NO_2 is oxidised by O_3 (R4). HNO_3 is
113 ultimately formed via the hydrolysis of dinitrogen pentoxide (N_2O_5), following the reactions (R5) and (R6) below:



117 NO_3 can also react with hydrocarbons (HC) (e.g., dimethylsulphide (DMS)) to form HNO_3 following reaction (R7) below:



119 Lastly, in regions with elevated halogen concentrations, NO_2 can be oxidised by reactive halogens, for example bromine oxide
120 (BrO), to form HNO_3 following (R8) and (R9) below:



123 Typically, aerosol $\delta^{18}\text{O}-\text{NO}_3^-$ is interpreted as being determined by the dominant NO_x oxidation pathways, (R3) versus
124 (R4) to (R9). If some combination of R4-R9 occurs, then O_3 is the main oxidant, whereas during (R3), one of the O atoms
125 originates from OH . The OH radical exchanges with H_2O vapor in the troposphere, therefore the $\delta^{18}\text{O}$ of OH is a function of
126 the $\delta^{18}\text{O}$ of H_2O vapour, which generally ranges from -27.5% to 0% in the subtropics and over the Southern Ocean (Michalski,
127 et al., 2012; Guilpart, et al., 2017; Dar, et al., 2020), and equilibrium isotope exchange between OH and H_2O (Walters &



128 Michalski, 2016). In contrast the $\delta^{18}\text{O}$ of tropospheric O_3 is much higher, the most recent estimate being $114.8 \pm 10.4\%$ (Vicars
129 & Savarino, 2014). Therefore, a higher $\delta^{18}\text{O}$ for atmospheric NO_3^- reflects the increased influence of O_3 on NO_x to NO_3^-
130 conversion (R4-R9), and the $\delta^{18}\text{O}-\text{NO}_3^-$ is lower when (R3) is favoured, due to the lack of exchange of O atoms with O_3
131 (Hastings, et al., 2003; Fang, et al., 2011; Altieri, et al., 2013).

132 Here, we present the concentration and isotopic composition of coarse mode ($> 1 \mu\text{m}$) atmospheric NO_3^- collected in the
133 MBL of the Southern Ocean between Cape Town, South Africa and coastal Antarctica, as well as across the Weddell Sea gyre,
134 during summer. Using air mass back trajectories, surface ocean nitrite measurements, and the aerosol $\delta^{15}\text{N}$ - and $\delta^{18}\text{O}-\text{NO}_3^-$,
135 we address 1) the major NO_x sources as well as the main oxidants in NO/NO_2 cycling and NO_x to NO_3^- conversion across a
136 large latitudinal transect of the Atlantic Southern Ocean and within the Weddell Sea gyre, and 2) the influence of sea-ice and
137 snowpack emissions on $\text{NO}_x/\text{NO}_3^-$ chemistry in the high-latitude MBL.

138 2) Methods

139 2.1) Sample collection

140 Samples were collected on board the Research Vessel (R/V) *SA Agulhas II* during one cruise subdivided into three legs. Leg
141 one refers to the voyage south from Cape Town (33.9°S , 18.4°E) to Penguin Bukta (71.4°S , 2.5°W) in early summer (7
142 December 2018 to 19 December 2018) as part of the South African National Antarctic Expedition's annual relief voyage
143 (SANAE 58). Leg two is the Weddell Sea Expedition (WSE) from 4 January 2019 to 21 February 2019. The WSE refers to
144 the voyage west from Penguin Bukta to the northern edge of the Weddell Sea gyre to Larsen C ice shelf, followed by a detour
145 to King George Island before returning to the Weddell Sea and sailing back to Penguin Bukta. Leg three refers to the SANAE
146 58 return voyage north from Penguin Bukta to Cape Town in late summer (27 February 2019 to 15 March 2019). From here
147 on legs one, two and three will be referred to as early summer, the Weddell Sea, and late summer, respectively.

148 Size-segregated atmospheric aerosols were collected on the ninth floor above the bridge (approximately 20 m above sea
149 level), using a high-volume air sampler (HV-AS; Tisch Environmental). Air was pumped at an average flow rate of 0.82 m^3
150 min^{-1} through a five-stage cascade impactor (TE-235; Tisch Environmental), loaded with combusted (400°C for 4 hours) glass
151 fibre filters. Aerosol nitrate in the MBL is predominantly present in the coarse mode ($> 1 \mu\text{m}$), therefore only filter stages 1
152 through 4 were analysed, where the aerodynamical diameter of particles collected are as follows: stage 1 ($> 7 \mu\text{m}$); stage 2 (3
153 to $7 \mu\text{m}$); stage 3 (1.5 to $3 \mu\text{m}$) and stage 4 (1 to $1.5 \mu\text{m}$).

154 A sector collector was used to restrict HV-AS activity to avoid contamination from ship stack emissions (Campbell
155 Scientific Africa). The HV-AS only began operating if the wind was blowing at an angle less than 75° or greater than 180°
156 from the bow of the ship for a minimum of ten minutes at a speed of at least 1 m s^{-1} . Filters were removed from the cascade
157 impactor inside a laminar flow cabinet (Air Science), placed in individual zip-sealed plastic bags and stored at -20°C until
158 analysis.



159 Given that the MBL of the Southern Ocean is characterised by low atmospheric NO_3^- concentrations, an attempt was made
160 to ensure that at least 24 hours of in-sector sampling had passed before filters were removed from the cascade impactor.
161 However, this was not always possible as on occasion the filters had to be removed early to avoid contamination due to unusual
162 ship manoeuvres resulting in stagnant conditions. Therefore, sampling times ranged between 13 and 88 hours across the three
163 legs. The details of each cruise leg can be found in the supplemental information (Table S1).

164 During the research voyage, a field blank was collected by fitting the cascade impactor with a set of filters and walking the
165 cascade impactor from the laboratory to the HV-AS in the same way that atmospheric samples were deployed. The cascade
166 impactor was placed into the HV-AS and then immediately removed without the HV-AS turning on, after which the filters
167 were removed from the cascade impactor and stored in the same manner as the atmospheric samples. All chemical analyses
168 performed on samples were also performed on the field blanks to assess possible contamination during filter deployment or
169 sample handling.

170 2.2) Sample analysis

171 Filter stages 1 to 4 were extracted using ultra-clean deionised water (DI) under a laminar flow cabinet (Air Science). The
172 extraction ratio was approximately 30 cm^2 of filter in 25 mL of DI. Extracts were immediately sonicated for one hour and then
173 stored at 4°C for at least 12 hours. Thereafter, extracts were filtered (0.2 μm) using an acid washed syringe into a clean 30 mL
174 HDPE bottle and stored at -20°C until analysis (Baker, et al., 2010).

175 Aerosol nitrate concentrations ($[\text{NO}_3^-]$) were determined using a Thermo Scientific Dionex Aquion Ion Chromatography
176 (IC) system equipped with an autosampler. The anion IC contained an AG22 RFIC 4 x 50 mm guard column and AG22 RFIC
177 4 x 250 mm analytical column. A six-point standard curve was run on each day of analysis (Dionex Seven Anion-II Standard)
178 and an R^2 value > 0.999 was required for sample analysis to proceed. Final $[\text{NO}_3^-]$ were corrected by subtracting the field
179 blanks, which had an average of 484.7 nmol NO_3^- per filter deployment. The pooled standard deviation (Sp) of four repeated
180 sample measurements for $[\text{NO}_3^-]$ was 0.3 $\mu\text{mol L}^{-1}$. A subset of aerosol samples was analysed for $[\text{NO}_3^-]$ using a Lachat
181 QuikChem® flow injection autoanalyzer (precision of $\pm 0.8 \mu\text{mol L}^{-1}$). For the subset of samples analysed using both
182 instruments, the average $[\text{NO}_3^-]$ measured using the Lachat QuikChem® flow injection autoanalyzer and the IC system is
183 reported.

184 Nitrogen and oxygen isotopic ratios were measured using the denitrifier method (Sigman, et al., 2001 and Casciotti, et al.,
185 2002). To determine the $^{15}\text{N}/^{14}\text{N}$ and $^{18}\text{O}/^{16}\text{O}$ of NO_3^- , a natural strain of denitrifying bacteria, *Pseudomonas aureofaciens*, that
186 lack the terminal nitrous oxide (N_2O) reductase enzyme were used to convert aqueous NO_3^- quantitatively to N_2O gas. The
187 product N_2O was analysed by continuous flow isotope ratio mass spectrometry (IRMS) using a Delta V Advantage IRMS
188 interfaced with an online N_2O extraction and purification system. Individual analyses were referenced to injections of N_2O
189 from a pure gas cylinder and then standardized through comparison to the international reference materials of IAEA-N3 and
190 USGS34 for $\delta^{15}\text{N}-\text{NO}_3^-$, and IAEA-N3, USGS34 and USGS35 for $\delta^{18}\text{O}-\text{NO}_3^-$ (Table S2) (Bohlke et al., 2003). The $^{15}\text{N}/^{14}\text{N}$ of
191 samples was corrected for the contribution of ^{17}O to the peak at mass 45 using an average reported $\Delta^{17}\text{O}$ value of 26‰ from



192 atmospheric nitrate collected in the Weddell Sea (Morin, et al., 2009). The pooled standard deviation for all measurements of
193 IAEA-N3 and USGS34 for $\delta^{15}\text{N-NO}_3^-$, and IAEA-N3, USGS34 and USGS35 for $\delta^{18}\text{O-NO}_3^-$ are reported (Table S2). All
194 samples were measured in triplicate in separate batch analyses. The pooled standard deviation from all replicate analyses of
195 samples was 0.25‰ for $\delta^{15}\text{N-NO}_3^-$ and 0.64‰ for $\delta^{18}\text{O-NO}_3^-$. The average $\delta^{15}\text{N-NO}_3^-$ and $\delta^{18}\text{O-NO}_3^-$ computed for each filter
196 deployment was weighted by the $[\text{NO}_3^-]$ observed for each stage and error was propagated according to standard statistical
197 practises (Table S3).

198 Seawater samples were collected in triplicate every two hours from the ships underway system (position at depth ± 5 m)
199 for the analysis of surface ocean nitrite concentrations ($[\text{NO}_2^-]$). $[\text{NO}_2^-]$ was analysed using the colorimetric method of Grasshof
200 et al. (1983) using a Thermo Scientific Genesys 30 visible spectrophotometer (detection limit of $0.05 \mu\text{mol L}^{-1}$).

201 2.6) Air mass back trajectory analysis

202 To determine the air mass source region for each aerosol sample, air mass back trajectories (AMBTs) were computed for each
203 hour in which the HV-AS was operational for at least 45 minutes of that hour. Given that the ship was moving, a different
204 date, time and starting location was used to compute each AMBT. An altitude of 20 m was chosen to match the height of the
205 HV-AS above sea level and 72-hour AMBTs were computed to account for the lifetime of NO_3^- in the atmosphere. All AMBTs
206 were computed with NOAA's Hybrid Single-Particle Lagrangian Integrated Trajectory model (HYSPPLIT v 4), using NCEP
207 Global Data Assimilation System (GDAS) output, which can be accessed at <http://www.arl.noaa.gov/ready/hysplit4.html>
208 (NOAA Air Resources Laboratory, Silver Spring, Maryland) (Stein, et al., 2015; Rolph, 2016).

209 3) Results

210 The coarse mode ($> 1 \mu\text{m}$ in diameter) aerosol $[\text{NO}_3^-]$ computed by summing the $[\text{NO}_3^-]$ of stages 1 through 4, ranged from
211 22.3 to 374.2 ng m^{-3} (Fig. 1A and Table 1). The mass-weighted $\delta^{15}\text{N}$ of coarse mode aerosol NO_3^- ranged from -43.1‰ to -
212 2.7‰ (Figs. 1B, 2 and Table 1). The highest nitrate concentrations occurred between 34°S and 45°S, and then decreased with
213 increasing latitude. Similarly, higher values characterized $\delta^{15}\text{N-NO}_3^-$ between 34°S and 45°S ($-4.5 \pm 1.6\text{‰}$), and then decreased
214 with increasing latitude. At the high-latitudes (south of 60°S), median values of 41.7 ng m^{-3} and -22.2‰ were observed for
215 nitrate concentration and $\delta^{15}\text{N}$, respectively. Coincident mass-weighted $\delta^{18}\text{O-NO}_3^-$ values ranged from 16.5‰ to 70‰ (Figs.
216 1C, 3 and Table 1). No latitudinal trend in $\delta^{18}\text{O-NO}_3^-$ was apparent, although distinctly low $\delta^{18}\text{O-NO}_3^-$ values were observed
217 in the Weddell Sea, as discussed in section 4.3 below. The difference between $\delta^{18}\text{O-NO}_3^-$ observed in the Weddell Sea (during
218 January to February) and $\delta^{18}\text{O-NO}_3^-$ observed at corresponding latitudes during the early and late summer transects is
219 statistically significant ($p\text{-value} < 0.05$). The early and late summer cruise transects were similar spatially in that both took
220 place along the same hydrographic line (i.e., the Good Hope line), apart from the deviation to South Georgia during late
221 summer (Fig. 2A & B). Even though the early and late summer cruise transects occurred in December and March, respectively,

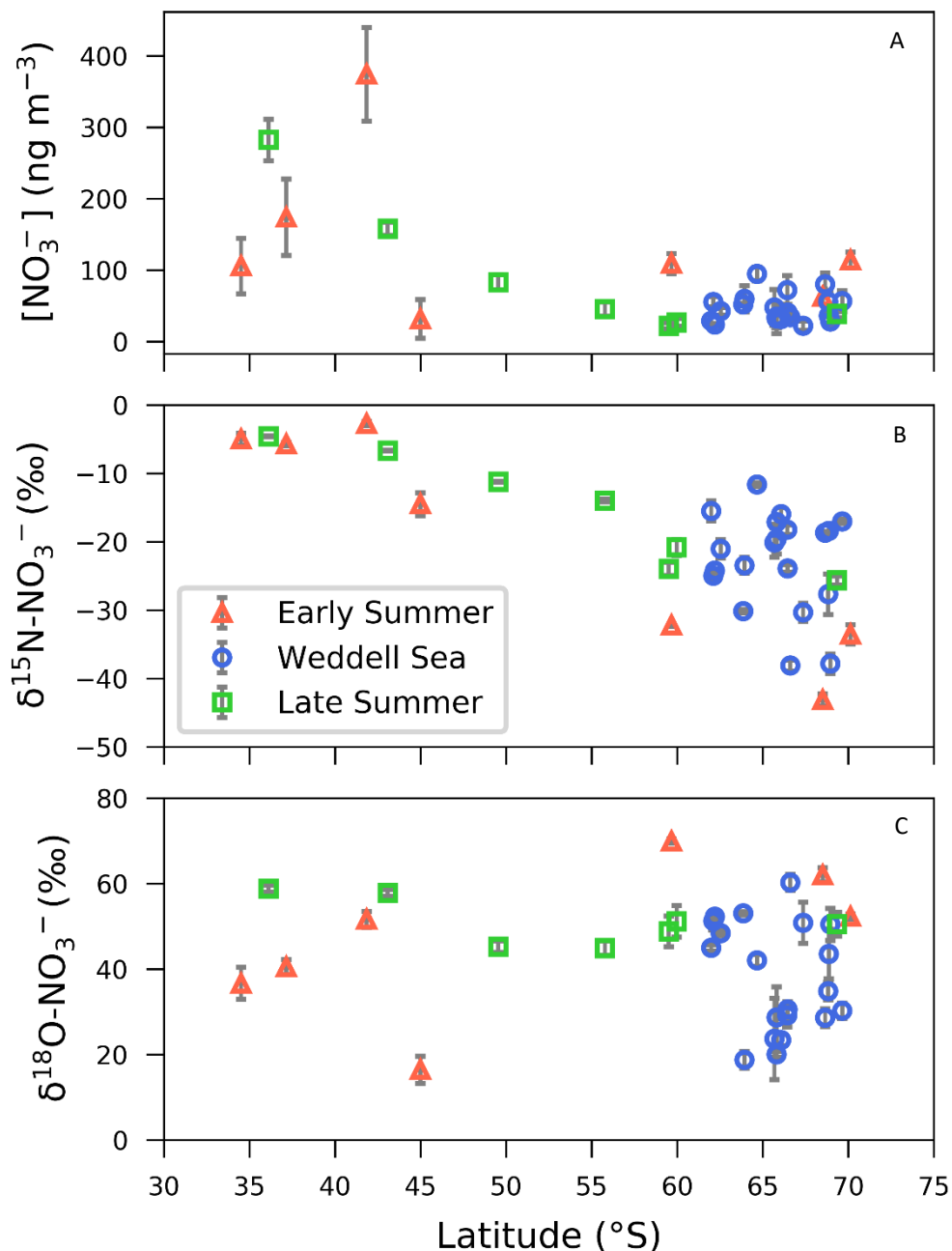


222 there is no statistically significant difference in $[\text{NO}_3^-]$, $\delta^{15}\text{N}\text{-NO}_3^-$ or $\delta^{18}\text{O}\text{-NO}_3^-$ between them ($p\text{-value} > 0.05$ in all cases).
223 Therefore, the early and late summer legs are discussed together and collectively referred to as the latitudinal transect.

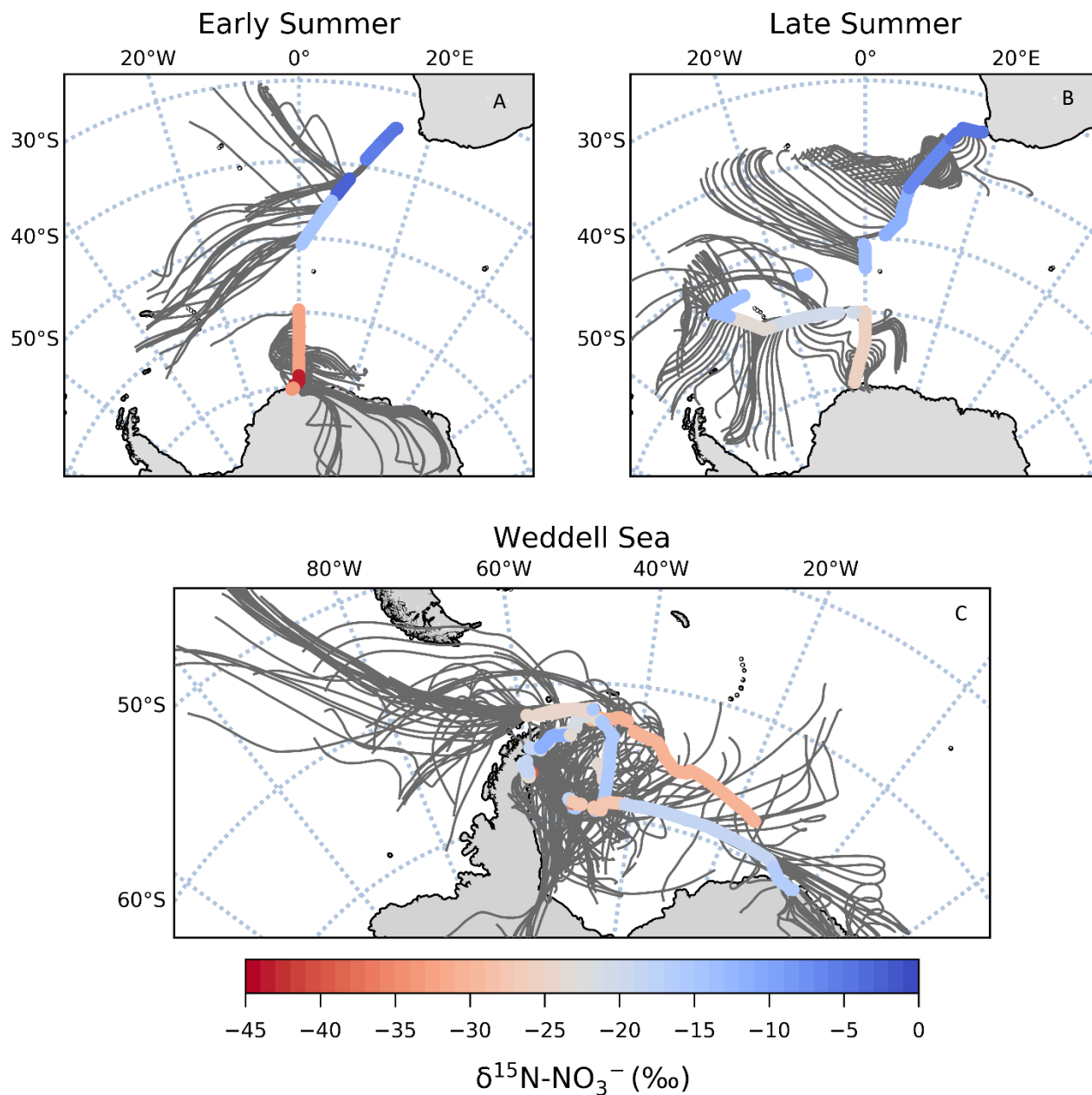
224

225 Table 1: The average (Avg), standard deviation (SD) and range of total coarse-mode ($> 1\mu\text{m}$) atmospheric nitrate
226 concentration ($[\text{NO}_3^-]$; ng m^{-3}) and the mass weighted average N and O isotopic composition of coarse mode nitrate ($\delta^{15}\text{N}\text{-}$
227 NO_3^- and $\delta^{18}\text{O}\text{-NO}_3^-$; ‰) are shown. Cruise legs are denoted as follows: early summer (ES), Weddell Sea (WS) and late
228 summer (LS).

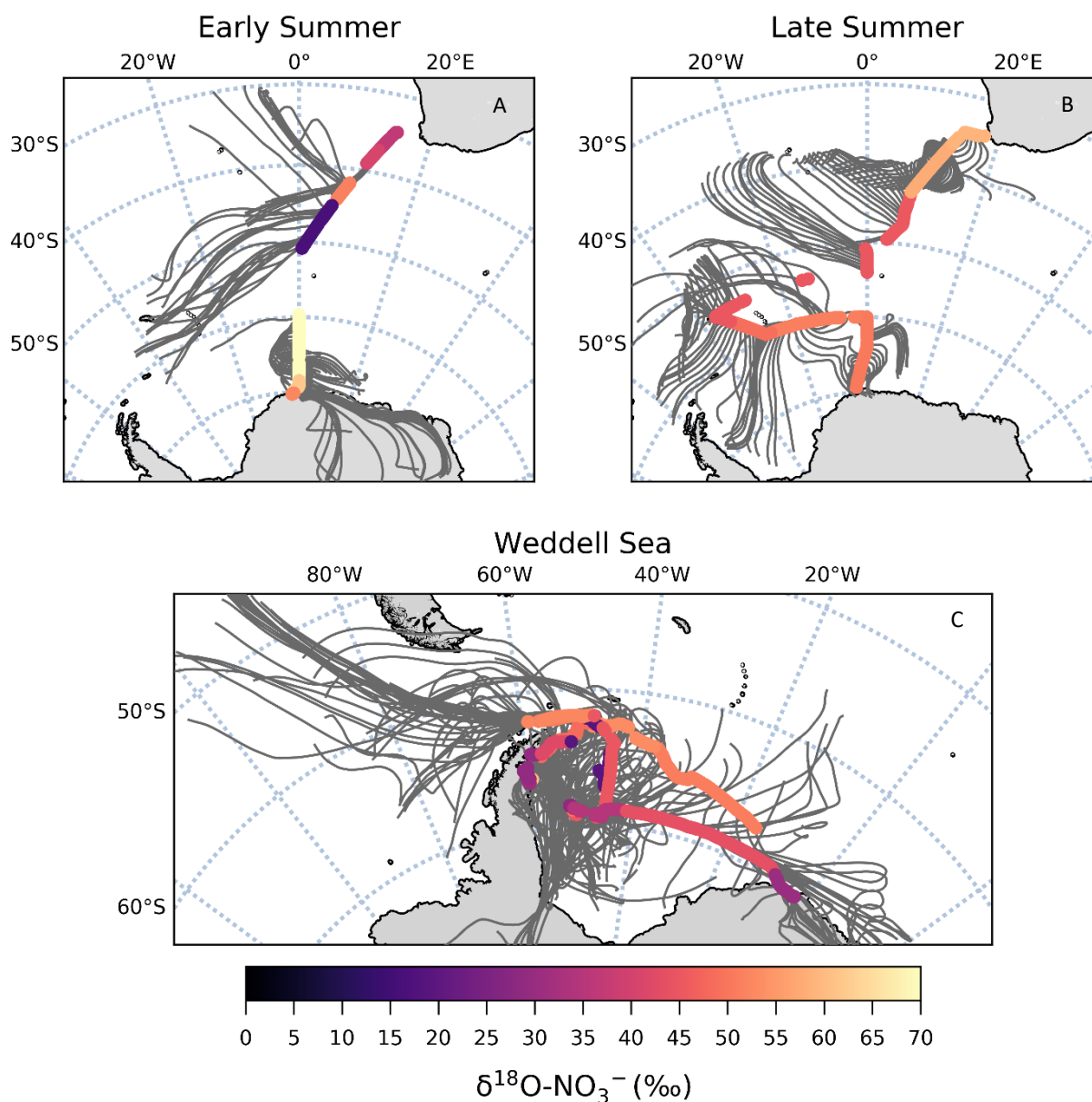
Leg	$[\text{NO}_3^-]$ (ng m^{-3})		$\delta^{15}\text{N}\text{-NO}_3^-$ (‰ vs. N_2)		$\delta^{18}\text{O}\text{-NO}_3^-$ (‰ vs. VSMOW)	
	Avg (SD)	Range	Avg (SD)	Range	Avg (SD)	Range
ES	139 (112.8)	31.9 to 374.2	-19.5 (16.4)	-43.1 to -2.7	47.1 (17.7)	16.5 to 70.0
WS	46.7 (19.5)	22.3 to 94.8	-22.7 (7.1)	-38.1 to -11.6	38.3 (12.8)	18.8 to 60.3
LS	94.0 (95.5)	22.3 to 282.5	-15.3 (8.4)	-25.6 to -4.6	51.1 (5.5)	44.9 to 58.9



229 Fig. 1. The average (± 1 SD) coarse mode ($> 1\ \mu m$) nitrate concentration $[NO_3^-]$ ($ng\ m^{-3}$; A), and the weighted average (\pm
230 1 SD) $\delta^{15}N$ (B) and $\delta^{18}O$ (C) of atmospheric nitrate ($\delta^{15}N-NO_3^-$ (‰ vs. N_2) and $\delta^{18}O-NO_3^-$ (‰ vs. V-SMOW), respectively),
231 as a function of latitude ($^\circ S$). Early and late summer latitudinal transects are denoted by the red triangles and green squares,
232 respectively. Weddell Sea samples are denoted by blue circles. Where error bars (± 1 SD) are not visible, the standard
233 deviation is smaller than the size of the marker.



234 Fig. 2. 72-hour AMBT's (grey lines) computed for each hour of the voyage when the HV-AS was operational for more
235 than 45 minutes of the hour during early summer (A), late summer (B), and in the Weddell Sea (C). The colour bar
236 represents the weighted average $\delta^{15}\text{N}$ of coarse mode ($> 1 \mu\text{m}$) atmospheric nitrate ($\delta^{15}\text{N-NO}_3^-$).



237 Fig. 3. 72-hour AMBT's (grey lines) computed for each hour of the voyage when the HV-AS was operational for more
238 than 45 minutes of the hour during early summer (A), late summer (B), and in the Weddell Sea (C). The colour bar
239 represents the weighted average $\delta^{18}\text{O}$ of coarse mode ($> 1 \mu\text{m}$) atmospheric nitrate ($\delta^{18}\text{O}-\text{NO}_3^-$).



240 4) Discussion

241 The sum of our observations reveals a latitudinal gradient in atmospheric NO_3^- concentration and $\delta^{15}\text{N}-\text{NO}_3^-$, which we
242 hypothesize may be attributed to the varying contribution of the dominant NO_x sources present between Cape Town and coastal
243 Antarctica. In contrast, $\delta^{18}\text{O}-\text{NO}_3^-$ depicts no latitudinal trend, however, very low $\delta^{18}\text{O}-\text{NO}_3^-$ values are observed in the Weddell
244 Sea, which we hypothesize may be attributed to the influence of sea ice emissions on NO_x cycling. Below, we first discuss the
245 extent to which anthropogenic NO_x sources may influence the observed atmospheric NO_3^- concentrations and $\delta^{15}\text{N}$ signatures.
246 Then we discuss the dominant NO_x sources to low, mid and high latitude Southern Ocean MBL NO_3^- , determined in part from
247 72-hour AMBT's, as well as the role of various oxidants in NO/NO_2 cycling and NO_2 oxidation.

248 4.1) Minimal influence of anthropogenic NO_x sources

249 Aerosol NO_3^- concentrations were low ($< 100 \text{ ng m}^{-3}$; Fig. 1A) for most air masses sampled along the latitudinal transect
250 and in the Weddell Sea, consistent with the expectation of minimal influence from anthropogenic NO_x sources. Interestingly,
251 NO_3^- concentrations were higher ($\pm 300 \text{ ng m}^{-3}$; Fig. 1A) in samples collected near the South African coast at the beginning of
252 the latitudinal transect (i.e., above 43°S). However, 72-hour AMBTs computed for all latitudinal transect samples indicate that
253 sampled air masses originated from over the South Atlantic sector of the Southern Ocean (Fig. 2A and 2B), with no continental
254 influence and limited opportunity for direct anthropogenic NO_x emissions to contribute to aerosol NO_3^- , assuming NO_3^- has a
255 lifetime of 72 hours (Alexander, et al., 2020). As such, the higher atmospheric NO_3^- concentrations observed near South Africa
256 are best explained by greater lightning NO_x production, which generally occurs between 40°S and the ITCZ during summer
257 (Nesbitt, et al., 2000; van der A, et al., 2008).

259 4.2) Interpretation of natural NO_x sources using the N isotopic composition of atmospheric NO_3^-

260 Aerosol $\delta^{15}\text{N}-\text{NO}_3^-$ ranged from -2.7‰ for low-latitude air masses to -43.1‰ for high-latitude air masses (including those
261 sampled in the Weddell Sea; Fig. 1B). As discussed in section 1.1, the $\delta^{15}\text{N}-\text{NO}_3^-$ reflects the $\delta^{15}\text{N}$ of the source NO_x plus any
262 isotopic fractionation imparted from NO/NO_2 cycling or NO_x to NO_3^- conversion. Similar to previous studies, we surmise that
263 NO_x equilibrium fractionation is unlikely to be relevant in our system, as NO_x concentrations are significantly lower than O_3
264 concentrations (Elliott, et al., 2007; Morin, et al., 2009; Walters, et al., 2016; Park, et al., 2018). Typical O_3 concentrations
265 observed at coastal sites in Antarctica are on the order of 20 ppbv (Nadzir, et al., 2018), whereas the sum of NO and NO_2 rarely
266 exceeds 40 pptv (Jones, et al., 2000; Weller, et al., 2002; Bauguitte, et al., 2012). Under these conditions NO_x isotopic exchange
267 occurs at a much slower rate than (R1) and (R2), such that little to no equilibrium isotope fractionation is expressed and the
268 $\delta^{15}\text{N}$ of the NO_3^- should reflect the $\delta^{15}\text{N}$ of the NO_x source (Walters, et al., 2016). Additionally, equilibrium isotope effects are
269 temperature dependent (increasing with decreasing temperature) and here ambient temperatures decline with increasing
270 latitude. Therefore, if equilibrium isotope fractionation were occurring during $\text{NO}-\text{NO}_2$ cycling and/or NO_x to NO_3^- conversion,

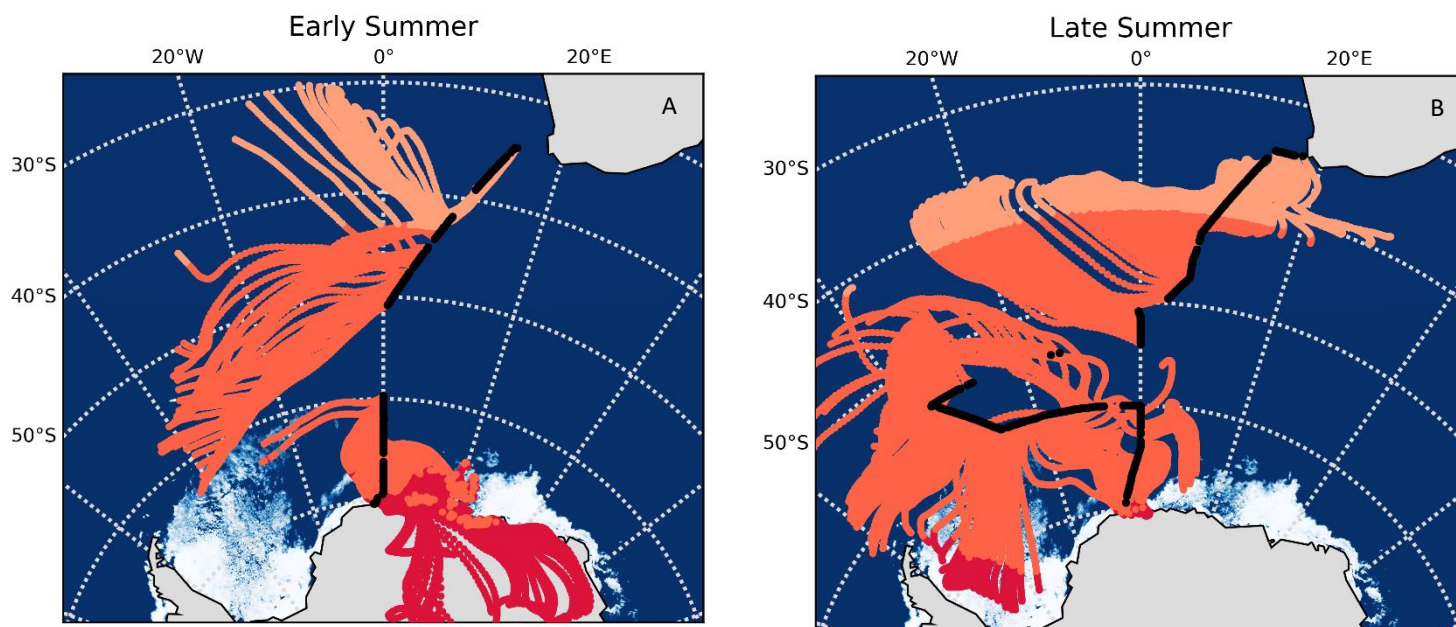


271 one would expect $\delta^{15}\text{N-NO}_3^-$ to increase with latitude, as both fractionation processes produce NO_3^- with a $\delta^{15}\text{N}$ signature
272 higher than the source NO_x . However, the opposite trend is observed here whereby $\delta^{15}\text{N-NO}_3^-$ decreases with increasing
273 latitude (Fig. 1B). Therefore, we discount the hypothesis that equilibrium isotope effects can explain the latitudinal gradient
274 in $\delta^{15}\text{N-NO}_3^-$.

275 NO_3^- in the Antarctic troposphere may also derive from stratospheric denitrification, whereby HNO_3 is injected into the
276 troposphere from the stratosphere via the subsidence and penetration of polar stratospheric clouds (PSC). However, this
277 phenomenon typically occurs in winter when the tropospheric barrier is weak and the lower stratosphere is cold enough for
278 PSC formation (Savarino, et al., 2007; Walters, et al., 2019). Furthermore, $\delta^{15}\text{N-NO}_3^-$ originating from stratospheric inputs is
279 estimated to be $19\% \pm 3\%$ (Savarino, et al., 2007), a value substantially greater than the atmospheric $\delta^{15}\text{N-NO}_3^-$ observed here
280 for high-latitude air masses; thus, we discount a direct influence from stratospheric NO_x . We propose that the observed
281 variation in atmospheric $\delta^{15}\text{N-NO}_3^-$ across the Southern Ocean is therefore best explained by the changing contribution of three
282 dominant NO_x sources: lightning, surface ocean alkyl nitrate emissions, and photochemical production on snow and ice,
283 determined using AMBT analyses and typical NO_x source signatures where possible, as discussed below.

284 4.2.1) High-latitudes: Photochemical NO_x source

285 Aerosol $\delta^{15}\text{N-NO}_3^-$ was very low in air masses from the southern high-latitudes, including in the Weddell Sea (average of
286 -24.3% ; Figs. 1B & 2). The latitudinal gradient in lightning suggests that NO_x production via this mechanism is greatly reduced
287 at high-latitudes (Savarino, et al., 2007). Similar to other studies in the region (Savarino, et al., 2007; Morin, et al., 2009), we
288 suggest that photochemical NO_x production on snow or ice accounts for the low aerosol $\delta^{15}\text{N-NO}_3^-$ in high-latitude air masses,
289 where high-latitude air mass samples are defined as those exposed to the Antarctic continent or the surrounding sea ice (with
290 sea ice concentration being at least 50%) (Fig. 4, red). Antarctic estimates for isotopic fractionation associated with snow NO_3^-
291 photolysis during summer range from -47.9% to -55.8% for laboratory and field experiments, respectively (Berhanu, et al.,
292 2014, 2015), resulting in the emission of low $\delta^{15}\text{N}$ NO_x to the overlying atmosphere (Savarino, et al., 2007; Morin, et al., 2009;
293 Shi, et al., 2018; Walters, et al., 2019). Therefore, NO_3^- photolysis explains the very low $\delta^{15}\text{N-NO}_3^-$ observed in high-latitude
294 air masses in early and late summer that crossed snow-covered continental ice or sea ice before being sampled (Figs. 2 and 4).
295 During early summer, air masses spent significantly more time over the snow-covered continent compared to late summer
296 (Figs. 2A & B) and the sea ice extent was greater in early summer compared to late summer (Fig. 4). Combined, these dynamics
297 resulted in a much lower $\delta^{15}\text{N-NO}_3^-$ for high-latitude air masses during early summer compared to late summer (minimum
298 value of -43.1% vs -25.6%). Similarly low MBL $\delta^{15}\text{N-NO}_3^-$ values ($< -30\%$) were recently observed for the southern high
299 latitudes of the Indian ocean (Shi, et al., 2021). Our data are also consistent with previous year-round studies of atmospheric
300 NO_3^- at coastal Antarctica (Savarino, et al., 2007) and the South Pole (Walters, et al., 2019), where $\delta^{15}\text{N-NO}_3^-$ was reported
301 to range from -46.9% to 10.8% and from -60.8% to 10.5% , respectively. Both studies observed a seasonal cycle in $\delta^{15}\text{N-}$
302 NO_3^- whereby the lowest values occurred during sunlit periods (i.e., summer) due to snowpack NO_x emissions and the highest
303 values occurred during dark periods (i.e., winter) due to stratospheric inputs (Savarino, et al., 2007; Walters, et al., 2019).



304 Fig. 4. 72-hour AMBT's computed for each hour of the voyage during early (A) and late (B) summer, when the HV-AS
305 was operational for more than 45 minutes of the hour. Light orange, dark orange and red AMBT's represent time spent over
306 the low, mid- and high latitude SO, respectively. The white represents the location of the sea-ice at the southernmost extent of
307 each transect. Satellite derived sea ice concentration was obtained from the AMSR2 ASI programme.

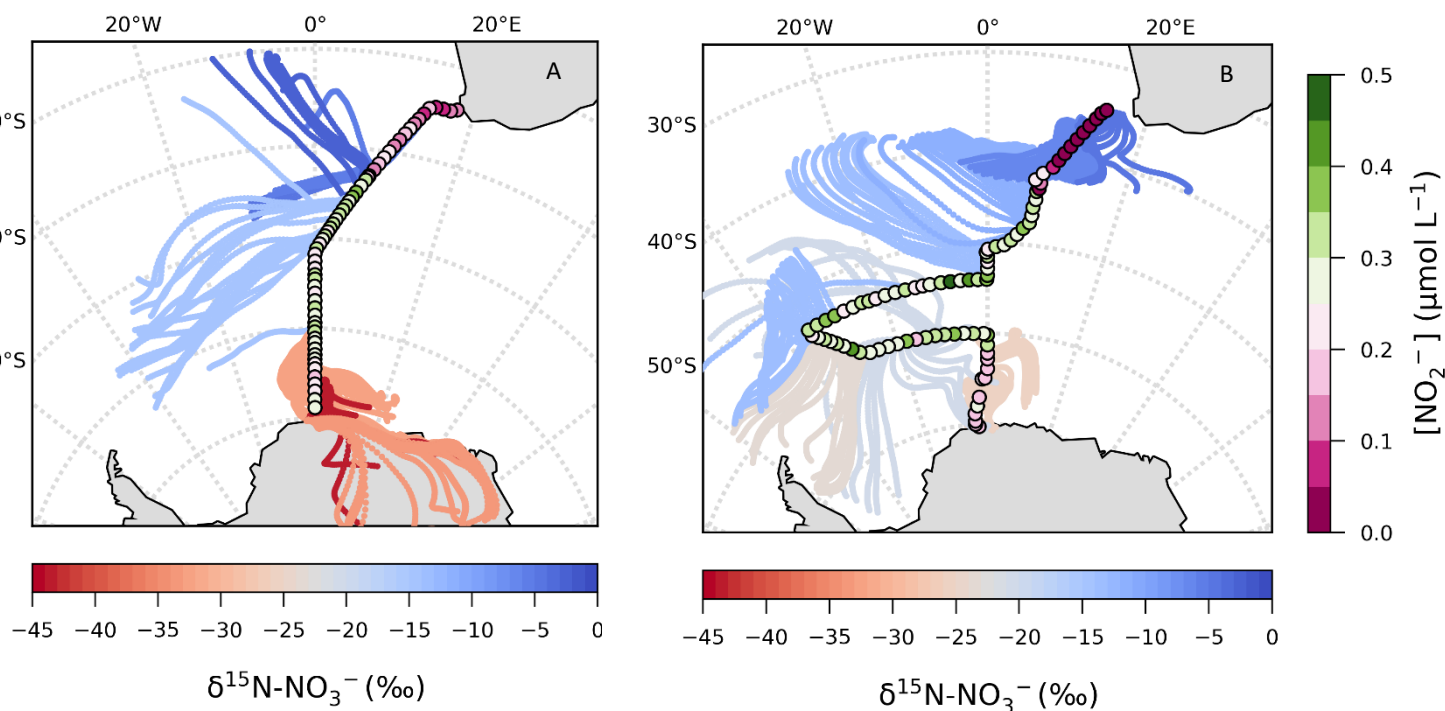
308 4.2.2) Low- to Mid-latitudes: Oceanic NO_x source

309 At the northern extent of our transects, the low-latitude aerosol samples, defined as those originating from anywhere north
310 of 43°S in early summer and 41°S in late summer (Fig. 4, light orange), had the highest average $\delta^{15}\text{N-NO}_3^-$ signature ($-4.9 \pm$
311 1.5‰ ; $n = 5$). These values can be attributed to lightning-generated NO_x, which has a $\delta^{15}\text{N}$ signature close to 0‰ (Hoering,
312 1957). Lightning activity at the low latitudes is also consistent with the higher atmospheric [NO₃⁻] observed (Fig. 1A). An
313 average atmospheric $\delta^{15}\text{N-NO}_3^-$ signature of -4‰ was previously reported for the low latitude Atlantic Ocean, between 45°S
314 and 45°N, and similarly attributed to a combination of natural NO_x sources including lightning (Morin, et al., 2009).

315 Aerosol samples across the mid-latitudes had an average $\delta^{15}\text{N-NO}_3^-$ of -13.2‰ (Figs. 1B & 2). Mid-latitude air masses are
316 defined as those originating from anywhere south of 43°S in early summer and south of 41°S in late summer that made no
317 contact with Antarctica or any surrounding sea ice (Fig. 4, dark orange), therefore these samples were unlikely to be influenced



318 by snow emitted NO_x with its light isotopic signature. The beginning of the mid-latitude zone (i.e., end of the low-latitude
319 zone) was defined by the presence of non-zero sea surface nitrite concentrations in early and late summer (Fig. 5). However,
320 the observed aerosol $\delta^{15}\text{N-NO}_3^-$ was too low (-14.5‰ to -11.2‰) to be explained solely by lightning generated NO_x . In the
321 absence of any signature of anthropogenic NO_x emissions (see Sect. 4.1), we argue that the dominant NO_x source for the mid-
322 latitude samples originates from seawater.



323 Fig. 5. 72-hour AMBT's computed for each hour of the voyage during early (A) and late (B) summer, when the HV-AS
324 was operational for more than 45 minutes of the hour. AMBT's are colour coded by the weighted average $\delta^{15}\text{N}$ of atmospheric
325 nitrate ($\delta^{15}\text{N-NO}_3^-$), represented by the horizontal colour bar. Over-layered are the surface ocean nitrite concentrations (circles;
326 $[\text{NO}_2^-]; \mu\text{mol L}^{-1}$), measured along each transect and represented by the vertical colour bar.

327
328 As mentioned in section 1, the most likely mechanism for an oceanic NO_x source is via the photolysis of surface ocean
329 derived RONO_2 in the MBL. NO derived from seawater nitrite is thought to limit RONO_2 production (dahl & Saltzman 2008;
330 Dahl et al., 2012), such that non-zero nitrite concentrations are required for RONO_2 production to occur. Here, surface ocean
331 nitrite concentrations were relatively high, in particular from $\sim 41^\circ\text{S}$ to 50°S (Fig. 5). Furthermore, the latitudinal extent of



332 mid-latitude air masses with low $\delta^{15}\text{N-NO}_3^-$ signatures corresponds well with the same latitudinal extent in which non-zero
333 surface ocean nitrite concentrations occurred (Figs. 4 and 5). As such, we suggest that in this region oceanic RONO_2 emission
334 is the main source to the Southern Ocean MBL, ultimately resulting in the low $\delta^{15}\text{N-NO}_3^-$ values observed for mid-latitude air
335 masses.

336 No estimates exist for the $\delta^{15}\text{N}$ of oceanic RONO_2 , however RONO_2 photolysis may yield isotopically light NO_x given that
337 NO_3^- photolysis produces low $\delta^{15}\text{N}$ products (e.g., Frey et al., 2009). Therefore, once oxidised in the overlying atmosphere,
338 NO_x derived from oceanic RONO_2 photolysis may form atmospheric NO_3^- with a low $\delta^{15}\text{N}$ signature. Aerosol $\delta^{15}\text{N-NO}_3^-$
339 values have been observed to range from -14.1‰ to -7.3‰ in the eastern equatorial Pacific (Kamezaki, et al., 2019) and from
340 -6‰ to ~0‰ (average = -3.4‰) in the western equatorial Pacific (Shi, et al., 2021). Observed $\delta^{15}\text{N-NO}_3^-$ is higher in the
341 western compared the eastern equatorial Pacific, which could be attributed to the proximity of the western equatorial Pacific
342 to continental/anthropogenic NO_x sources, resulting in NO_3^- having a higher $\delta^{15}\text{N}$ signature. The low average $\delta^{15}\text{N-NO}_3^-$
343 observed for the mid-latitude air masses of the Southern Ocean MBL sampled in the present study (-14.5‰ to -11.2‰), are
344 remarkably similar to those observed in the eastern equatorial Pacific (Kamazaki, et al., 2019). Kamezaki et al., (2019) also
345 concluded that such low $\delta^{15}\text{N-NO}_3^-$ values cannot be explained solely by lightning NO_x and given the lack of considerable
346 influence from any continental NO_x sources, they invoked the contribution of oceanic N emissions in the form of ammonia
347 (NH_3) and/or RONO_2 . However, NH_3 flux data for the summertime Atlantic Southern Ocean derived from in situ
348 ocean/atmosphere observations suggest that the ocean in this region is a net sink of NH_3 (Altieri, et al., 2021).

349 The latitudinal extent of our sampling campaign enabled us to estimate a range of likely values for the N isotopic
350 composition of NO_3^- derived from oceanic RONO_2 . We split the latitudinal transect into three regions, each characterised by
351 the dominance of a different natural source of NO_3^- i.e., lightning NO_x at the low-latitudes, oceanic RONO_2 emissions at the
352 mid-latitudes and snowpack emissions at the high-latitudes. Assuming that the dominant natural source of NO_3^- is the only
353 source relevant in each latitudinal zone, we estimate the contribution of each source to total NO_3^- formation by ascertaining
354 the amount of time air masses spent in each zone. We further assume that atmospheric $\delta^{15}\text{N-NO}_3^-$ reflects at most a combination
355 of two sources based on the AMBTs of each sample, either lightning NO_x and oceanic RONO_2 emissions near South Africa,
356 or oceanic RONO_2 emissions and snowpack NO_x emissions near Antarctic (Fig. 4 and Table S4). Using a two-end member
357 mixing model the $\delta^{15}\text{N}$ signature of the source NO_3^- derived from mid-latitude Southern Ocean RONO_2 emissions was
358 calculated for all samples where air masses from the mid-latitude region contributed at least 10% (Table S4). This 10%
359 threshold was chosen as the isotopic endmember of oceanic RONO_2 is harder to determine with confidence when its
360 contribution to total NO_3^- is less than 10%. For example, the AMBT's for sample ES 4 spent 3% of the time in the low-latitude
361 zone and 97% in the mid-latitude zone. Therefore, assuming lightning NO_x has a $\delta^{15}\text{N}$ signature of 0‰ and the measured $\delta^{15}\text{N-}$
362 NO_3^- for ES 4 is -14.5‰, we calculate the $\delta^{15}\text{N}$ signature of the RONO_2 -derived NO_3^- to be -14.9‰.

363 Using this approach for each filter deployment along the latitudinal transect, an average $\delta^{15}\text{N-NO}_3^-$ from oceanic RONO_2
364 emissions of $-22.0 \pm 7.5\%$ was estimated. Furthermore, the contribution of RONO_2 emissions can explain the lowering of
365 $\delta^{15}\text{N}$ from 0‰ for the low-latitude air mass samples. For example, the highest $\delta^{15}\text{N}$ observed in the study was -2.7‰, and this



366 sample has a < 5% contribution from the mid-latitude zone. The other two low-latitude samples have 30% to 40% contribution
367 from the mid-latitude zone and their $\delta^{15}\text{N}$ is lower (Table S3), as expected due to the influence of RONO_2 emissions. The
368 influence of low $\delta^{15}\text{N}\text{-NO}_3^-$ from RONO_2 emissions is not limited to the Southern Ocean, and this estimate of the N isotopic
369 composition for the RONO_2 derived NO_3^- source may be useful to constrain the contribution of RONO_2 emissions to NO_3^-
370 formation in other ocean regions with elevated surface ocean nitrite concentrations, such as the tropical Pacific.

371 4.3) The O isotopes of atmospheric nitrate

372 The corresponding $\delta^{18}\text{O}$ values allow us to determine the pathways of NO_3^- formation from NO_x . However, an assumption
373 must first be made regarding the oxidation of NO to NO_2 . While the dominant oxidant of NO to NO_2 is O_3 (R1) in most of the
374 troposphere, over the open ocean there can be a significant contribution via the reaction of NO with peroxy radicals (HO_2 and
375 its organic homologues RO_2) (Alexander et al., 2020). Peroxy radicals compete with O_3 to convert NO into NO_2 via R10:



377 The $\delta^{18}\text{O}$ of peroxy radicals is much lower than that of O_3 because the O atoms derive from atmospheric O_2 , which has a well-
378 defined $\delta^{18}\text{O}$ of 23.9‰ (Kroopnick & Craig, 1972). The $\delta^{18}\text{O}\text{-NO}_2$ can then be calculated using equation 2,

$$379 \delta^{18}\text{O}\text{-NO}_2 = (\delta^{18}\text{O}\text{-O}_2)(1-f) + (\delta^{18}\text{O}\text{-O}_3^*)(f) \quad (2)$$

380 where f is the fraction of NO_2 formed from R1, (1-f) is the fraction formed from R10, and the terminal $\delta^{18}\text{O}\text{-O}_3$ value ($\delta^{18}\text{O}\text{-O}_3^*$)
381 is $130.4 \pm 12.9\text{‰}$ (Vicars & Savarino, 2014).

382 The $\delta^{18}\text{O}\text{-NO}_3^-$ is then determined using equation 3 in which two thirds of the O atoms in NO_3^- come from NO_2 and one
383 third comes from OH i.e., R3, or using equation 4 in which three sixths of the O atoms in NO_3^- come from O_3 , two sixths come
384 from NO_2 and one sixth comes from H_2O i.e., R4-R6 (Hastings, et al., 2003; Alexander, et al., 2020).

$$385 \delta^{18}\text{O}\text{-NO}_3^-(\text{R3}) = (2/3)(\delta^{18}\text{O}\text{-NO}_2) + (1/3)(\delta^{18}\text{O}\text{-OH}) \quad (3)$$

$$386 \delta^{18}\text{O}\text{-NO}_3^-(\text{R4-R6}) = (1/2)(\delta^{18}\text{O}\text{-O}_3^*) + (1/3)(\delta^{18}\text{O}\text{-NO}_2) + (1/6)(\delta^{18}\text{O}\text{-H}_2\text{O}) \quad (4)$$

387 We assume that 15% of NO to NO_2 conversion occurs via HO_2/RO_2 oxidation and 85% by O_3 oxidation as is suggested by
388 global models (Alexander, et al., 2020), and use the minimum and maximum $\delta^{18}\text{O}\text{-H}_2\text{O}$ range of -27.5‰ to 0‰, the
389 temperature-dependent equilibrium isotope exchange between OH and H_2O (Walters & Michalski, 2016), and the resulting
390 minimum and maximum estimates for $\delta^{18}\text{O}\text{-OH}$ of -67.4‰ to -41.0‰. Using these assumptions and equations 3 and 4, the
391 expected $\delta^{18}\text{O}\text{-NO}_3^-$ for the daytime OH oxidation pathway (R3) is 46.5‰ to 71.4‰, and for the dark reactions (R4-R6) is
392 88.7‰ to 113.5‰. The observed $\delta^{18}\text{O}\text{-NO}_3^-$ values were all less than 70‰ (Figs. 1C and 3), suggesting that NO_x oxidation by
393 OH (R3) was indeed the dominant pathway for atmospheric NO_3^- formation during summer. The low $\delta^{18}\text{O}\text{-NO}_3^-$ values
394 observed suggest a minimal influence of O_3 in the oxidation chemistry, ruling out both the halogen (R8 to R9) and DMS (R7)
395 related NO_3^- formation pathways in addition to N_2O_5 hydrolysis (R4-6). This is consistent with previous year-round studies of
396 atmospheric NO_3^- at coastal Antarctica (Savarino, et al., 2007) and the South Pole (Walters, et al., 2019) where $\delta^{18}\text{O}\text{-NO}_3^-$ was
397 at a minimum in summer (59.6‰ and 47.0‰, respectively). Both studies confirm the importance of HO_x oxidation chemistry



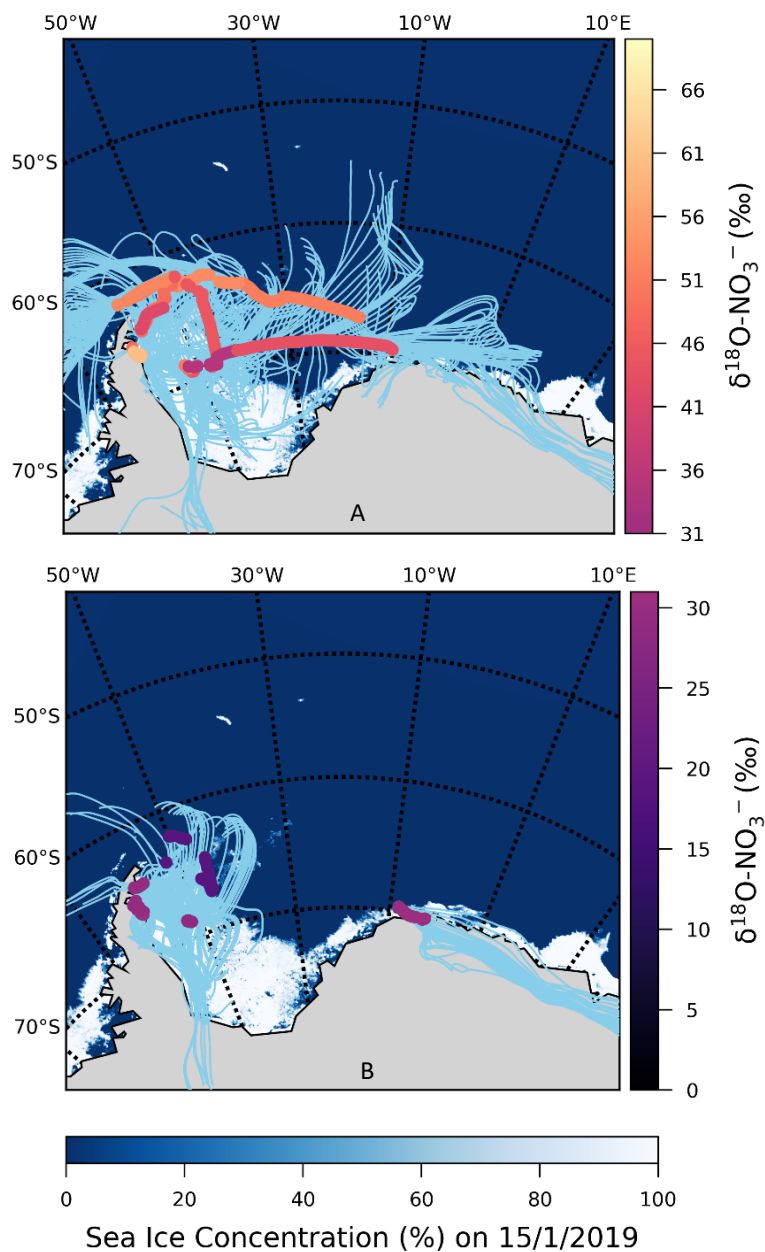
398 in summer when solar radiation enhances the production of these oxidants, followed by a switch to O₃ dominated oxidation
399 chemistry in winter (Savarino, et al., 2007; Ishino, et al., 2017; Walters, et al., 2019).

400 Interestingly, most aerosol samples have a δ¹⁸O-NO₃⁻ less than 46.5‰ (n=18), the lower limit estimated above for the OH
401 pathway. This suggests that there is more NO to NO₂ conversion via HO₂/RO₂ oxidation occurring than the global average. A
402 maximum HO₂/RO₂ contribution to NO oxidation of ~63% is required to explain the lowest δ¹⁸O-NO₃⁻ value, which was
403 observed over the mid-latitudes during early summer. Increased RO₂ production over the mid-latitudes could derive from
404 RONO₂ photolysis in the MBL, which we hypothesize is happening in this region based on the δ¹⁵N-NO₃⁻ (Section 4.2.2).
405 Although the lowest δ¹⁸O observation occurred in the mid-latitudes, the majority of low δ¹⁸O-NO₃⁻ values were observed in
406 the Weddell Sea, away from the region of maximum RONO₂ emissions. Approximately half of the Weddell Sea samples have
407 a δ¹⁸O-NO₃⁻ < 31‰, which would require a HO₂/RO₂ contribution to NO oxidation upwards of 40% (more than double the
408 contribution estimated by global models (Alexander, et al., 2020)). These δ¹⁸O-NO₃⁻ observations are unusually low compared
409 to previous observations for the same region in spring (Morin, et al., 2009). We hypothesize that the large contribution of
410 HO₂/RO₂ to NO/NO₂ oxidation (i.e., a decrease in f in equation 2) resulting in these low δ¹⁸O-NO₃⁻ values is due to the
411 influence of sea ice emissions. The 72-hour AMBTs for these low δ¹⁸O-NO₃⁻ Weddell Sea samples indicate that all the air
412 masses either originated from, or spent a significant amount of time recirculating, over the sea ice covered region of the western
413 Weddell Sea (Fig. 6A). By contrast, aerosol samples from the Weddell Sea with δ¹⁸O-NO₃⁻ values greater than 31‰ have air
414 masses that experienced significantly more oceanic influence (Fig. 6A). There is evidence that sea ice can lead to enhanced
415 peroxy radical production (Brough et al., 2019). In that work, increased HO₂ + RO₂ concentrations were observed during
416 spring at a coastal Antarctic site when air masses arrived from across a sea ice covered zone. This was attributed to the oxidation
417 of hydrocarbons by chlorine atoms, which leads to increased RO₂ concentrations via R11 and R12:





420
421
422
423
424
425
426
427
428
429
430
431
432
433
434
435
436
437
438
439
440
441
442
443
444
445
446
447
448



449 Fig. 6. 72-hour AMBT's (light blue dashed lines) computed for each hour of the voyage in the Weddell Sea, when the HV-
450 AS was operational for more than 45 minutes of the hour. The vertical colour bar represents the weighted average $\delta^{18}\text{O}$ of
451 atmospheric nitrate ($\delta^{18}\text{O}-\text{NO}_3^-$), where $\delta^{18}\text{O}-\text{NO}_3^-$ was $> 31\text{‰}$ (A) and $< 31\text{‰}$ (B). The horizontal colour bar represents
452 satellite derived sea ice concentration (%) for the 15th of January 2019, which corresponds to midway through the WS sampling
453 period. Satellite derived sea ice concentration was obtained from the AMSR2 ASI programme.



454

455 Cl atoms are much more reactive with hydrocarbons than OH (Monks, 2005) and can enhance hydrocarbon oxidation even
456 when present at low concentrations. Brough et al. (2019) suggest that air masses that traversed the sea ice zone contained
457 photolabile chlorine compounds that built up at night until photolysis occurred during the next day (Brough, et al., 2019).
458 Although our study was conducted in summer (the season of minimum sea ice extent), the sampling locations were uniquely
459 positioned at the western edge of the Weddell Sea gyre where significant sea ice remained (Fig. 6). Therefore, we suggest that
460 chlorine chemistry over the sea ice increased RO₂ concentrations at the time of our sampling, allowing the NO + RO₂ pathway
461 to play a more significant role in the Weddell Sea and resulting in low δ¹⁸O-NO₃⁻ values. We note that the only other estimates
462 of δ¹⁸O-NO₃⁻ from the Weddell Sea ranged from ~ 50‰ to 110‰ during springtime, and these samples were associated with
463 air masses that spent almost no time over the sea ice and therefore had limited potential for this peroxy radical chemistry to
464 drive down the δ¹⁸O-NO₃⁻ to the low values we observed (Morin, et al., 2009).

465 5) Conclusions

466 Our observations across a large latitudinal gradient of the summertime Southern Ocean MBL suggest it is dominated by natural
467 NO_x sources with unique isotopic signatures. Aerosol NO₃⁻ was predominantly formed from lightning generated NO_x with a
468 δ¹⁵N of ~ 0‰ at the lower latitudes, whereas snowpack NO_x emissions with a δ¹⁵N ~ -48‰ dominated the MBL inventory at
469 higher latitudes. Over the mid-latitudes, NO₃⁻ derived primarily from oceanic RONO₂ emissions, with an estimated δ¹⁵N
470 signature of ~ -22.0‰. This estimate may be valuable in constraining the contribution of oceanic RONO₂ emissions to NO₃⁻
471 formation in other ocean regions where this source has been invoked, such as the tropical Pacific (Kamezaki et al., 2019). The
472 isotopic composition of NO₃⁻ observed here can further inform interpretations of Antarctic ice core NO₃⁻ isotope records to
473 understand aerosol climate forcing and controls on the atmospheric oxidation budget over millennia (Freyer, et al., 1996; Jiang,
474 et al., 2019) – the interpretation of which relies on knowledge of the NO_x isotopic source signatures in the polar atmosphere.

475 The δ¹⁸O-NO₃⁻ values were consistently lower than 70‰, which confirms NO_x oxidation by OH (R3) to be the dominant
476 pathway for atmospheric NO₃⁻ formation during summer. However, unusually low δ¹⁸O-NO₃⁻ values observed at the mid-
477 latitudes and in the Weddell Sea indicate the increased importance of peroxy radicals (and decreased importance of O₃) in NO
478 oxidation to NO₂. At the mid-latitudes peroxy radicals (RO₂) may derive from RONO₂ photolysis in the MBL, while In the
479 Weddell Sea, sea ice appears to play an important role in the formation of this oxidant via its influence on chlorine chemistry
480 in the MBL (Brough, et al., 2019). This implies that snow covered sea ice is not only a source of NO_x but also other species
481 that have the potential to change the composition of the atmosphere above the ice and impact NO_x oxidation chemistry. These
482 results also highlight the utility of δ¹⁸O-NO₃⁻ to identify the major oxidants in NO oxidation, as well as NO_x to NO₃⁻ conversion.
483 In particular, δ¹⁸O-NO₃⁻ can serve as a useful tool for testing our understanding of the relative importance of HO₂/RO₂ in
484 NO/NO₂ cycling, which can be difficult to constrain in some environments.



485 Our study challenges the traditional paradigm that considers the ocean as a passive recipient of N deposition, as the
486 Southern Ocean mid-latitude NO_3^- source may derive almost entirely from oceanic RONO_2 emissions. In the tropical equatorial
487 Pacific atmosphere, Kamezaki et al. (2019) also suggested evidence for a low $\delta^{15}\text{N}$ - NO_3^- source derived from the ocean. In the
488 subtropical Atlantic Ocean MBL, Altieri et al. (2016) found that biogeochemical cycling in the surface ocean can directly
489 influence the lower atmosphere serving as a source of aerosol organic N and ammonium. This study suggests that the surface
490 waters of the Southern Ocean may also serve as a NO_x source, ultimately resulting in NO_3^- aerosol formation. As such, the
491 surface ocean may play a bigger role in atmospheric oxidative capacity over remote marine regions than previously thought.

492

493 *Author contributions.* K.E.A designed the study and sampling campaign, acquired funding and supervised the research. K.E.A
494 and J.G. provided financial and laboratory resources and assisted in data validation. K.A.M.S. and J.M.B conducted the
495 sampling at-sea and J.M.B. performed the laboratory analyses. M.G.H and E.J. assisted in data validation, reviewing, and
496 editing the manuscript. J.M.B analysed the data and prepared the manuscript with contributions from all co-authors.

497

498 *Competing interests.* The authors declare that they have no conflict of interest.

499

500 *Data availability statement.* Data sets for this research are available at [10.5281/zenodo.5006983](https://zenodo.org/record/5006983)

501

502 *Acknowledgements.* We thank the Captain and crew of the R/V *SA Agulhas II* for their support at sea and the Marine
503 Biogeochemistry Lab in the Oceanography Department at the University of Cape Town for their assistance in the field and
504 laboratory. We thank Lija Treibergs, Reide Jacksin and Peter Ruffino for their assistance in analysing the nitrate isotopes and
505 Riesna Audh for her assistance with satellite derived sea ice concentration data. We thank Riesna Audh, Raquel Flynn and
506 Shantelle Smith for nitrite concentration measurements, and Raquel Flynn for quality controlling the nitrite concentration data.
507 This research was partially funded by a CAREER award to JG from the U.S. National Science Foundation (OCE-1554474).
508 This research was also supported by the South African National Research Foundation through a Competitive Support for Rated
509 Researchers Grant to K.E.A. (111716), South African National Antarctic Programme Postgraduate Fellowship to J.M.B, and
510 Grant to K.E.A (110732); UCT support to K.E.A. through a University Research Council Launching Grant and VC Future
511 Leaders 2030 Grant.

512 **6) References**

513 Alexander, B., & Mickley, L. J.: Paleo-perspectives on the potential future changes in the oxidative capacity of the atmosphere
514 due to climate change and anthropogenic emissions, *Current Pollution Reports.*, 1, 57-69, DOI 10.1007/s40726-015-
515 0006-0, 2015.



- 516 Alexander, B., Sherwen, T., Holmes, C. D., Fisher, J. A., Chen, Q., Evans, A. J., Kasibhatla, P.: Global inorganic nitrate
517 production mechanisms: comparison of a global model with nitrate isotope observations. *Atmospheric Chemistry and*
518 *Physics*, 20(6), 3859-3877, <https://doi.org/10.5194/acp-20-3859-2020>, 2020.
- 519 Altieri, K. E., Fawcett, S. E., & Hastings, M.G.: Reactive Nitrogen Cycling in the Atmosphere and Ocean, *Annual Review of*
520 *Earth and Planetary Sciences*, 49, 513-540, <https://doi.org/10.1146/annurev-earth-083120-052147>, 2021.
- 521 Altieri, K. E., Fawcett, S. E., Peters, A. J., Sigman, D. M., & Hastings, M. G.: Marine biogenic source of atmospheric organic
522 nitrogen in the subtropical North Atlantic, *PNAS.*, 113(4), 925-930, <https://doi.org/10.1073/pnas.1516847113>, 2016
- 523 Altieri, K. E., Hastings, M. G., Gobel, A. R., Peters, A. J., & Sigman, D. M.: Isotopic composition of rainwater nitrate at
524 Bermuda: the influence of air mass source and chemistry in the marine boundary layer, *Journal of Geophysical*
525 *Research: Atmospheres*, 118, 11304-11316, <https://doi.org/10.1002/jgrd.50829>, 2013.
- 526 Atlas, E., Pollock, W., Greenberg, J., Heidt, L., & Thompson, A. M.: Alkyl nitrates, nonmethane hydrocarbons, and
527 halocarbon gases over the equatorial Pacific ocean during Saga 3, *Journal of Geophysical Research Letters*, 98(D9),
528 16933-16947, <https://doi.org/10.1029/93JD01005>, 1993.
- 529 Baker, A. R., Lesworth, T., Adams, C., Jickells, T. D., & Granzveld, L.: Estimation of atmospheric nutrient inputs to the
530 Atlantic Ocean from 50°N to 50°S based on large-scale field sampling: Fixed nitrogen and dry deposition of
531 phosphorus, *Global Biogeochemical Cycles*, 24, GB3006, <https://doi.org/10.1029/2009GB003634>, 2010.
- 532 Bauguitte, A. J.-B., Bloss, W. J., Evans, M. J., Salmon, R. A., Anderson, P. S., Jones, A. E., Lee, J. D., Saiz-Lopez, A., Roscoe,
533 H. K., Wolff, E. W., & Plane, J. M. C.: Summertime NO_x measurements during the CHABLIS campaign: can source
534 and sink estimates unravel observed diurnal cycles?, *Atmospheric Chemistry and Physics*, 12, 989-1002,
535 <https://doi.org/10.5194/acp-12-989-2012>, 2012.
- 536 Behrenfeld, M. J., Boss, E., Siegel, D. A., Shea, D. M.: Carbon-based ocean productivity and phytoplankton physiology from
537 space, *Global Biogeochemical Cycles*, 19(1), 1-14, <https://doi.org/10.1029/2004GB002299>, 2005.
- 538 Berhanu, T. A., Meusinger, C., Erbland, J., Jost, R., Bhattacharya, S. K., Johnson, M. S., & Savarino, J.: Laboratory study of
539 nitrate photolysis in Antarctic snow. II. Isotopic effects and wavelength dependence, *The Journal of Chemical*
540 *Physics*, 140(244306), 1-14, <https://doi.org/10.1063/1.4882899>, 2014.
- 541 Berhanu, T. A., Savarino, J., Erbland, J., Vicars, W. C., Preunkert, S., Martins, J. F., & Johnson, M. S.: Isotopic effects of
542 nitrate photochemistry in snow: a field study at Dome C, Antarctica, *Atmospheric Chemistry and Physics*, 15, 11243-
543 11256, <https://doi.org/10.5194/acp-15-11243-2015>, 2015.
- 544 Blake, N. J., Blake, D. R., & Swanson, A. L., Atlas, E., Flocke, F., & Rowland, F. S.: Latitudinal, vertical, and seasonal
545 variations of C1-C4 alkyl nitrate in the troposphere over the Pacific Ocean during PEM-Tropics A and B: Oceanic
546 and continental sources, *Journal of Geophysical Research Letters*, 108(D2), 1-14, doi:10.1029/2001JD001444, 2003.
- 547 Blake, N. J., Blake, D. R., Wingenter, O. W., Sive, B. C., Kang, C. H., Thornton, D. C., Bandy, A. R., Atlas, E., Flocke, F.,
548 Harris, J. M., & Rowland, F. S.: Aircraft measurements of the latitudinal, vertical, and seasonal variations of NMHCs,



- 549 methyl nitrate, methyl halides, and DMS during the First Aerosol Characterization Experiment (ACE 1), *Journal of*
550 *Geophysical Research Letters*, 104(D17), 21803-21817, 1999.
- 551 Böhlke, J. K., Mroczkowski, S. J., & Coplen, T. B.: Oxygen isotopes in nitrate: new reference materials for ^{18}O : ^{17}O : ^{16}O
552 measurements and observations on nitrate-water equilibrium, *Rapid Communications in Mass Spectrometry*, 17(16),
553 1835-1846, <https://doi.org/10.1002/rcm.1123>, 2003.
- 554 Brough, N., Jones, A. E., & Griffiths, P. T.: Influence of sea ice-derived halogens on atmospheric HO_x as observed in
555 Springtime coastal Antarctica, *Geophysical Research Letters*, 46, 10168-10176, <https://doi.org/10.1029/2019GL083825>, 2019.
- 556 Casado, M., Landais, A., Masson-Delmotte, V., Genthon, C., Kerstel, E., Kassi, S., Arnaud, L., Picard, G., Prie, F., Cattani,
557 O., Steen-Larsen, H. -C., Vignon, E., & Cermak, P.: Continuous measurements of isotopic composition of water
558 vapour on the East Antarctic Plateau, *Atmospheric Chemistry and Physics*, 16(13), 8521-8538,
559 <https://doi.org/10.5194/acp-16-8521-2016>, 2016.
- 560 Casciotti, K.L., Sigman, D.M., Hastings, M.G., Böhlke, J.K. & Hilkert, A.: Measurement of the oxygen isotopic composition
561 of nitrate in seawater and freshwater using the denitrifier method, *Analytical chemistry*, 74(19), 4905-4912,
562 <https://doi.org/10.1021/ac020113w>, 2002.
- 563 Chuck, A. L., Turner, S. M., & Liss, P. S.: Direct evidence for a marine source of C_1 and C_2 alkyl nitrates, *Science*, 297, 1151-
564 1154, <https://doi.org/10.1126/science.1073896>, 2002.
- 565 Dahl, E. E., & Saltzman, S. E.: Alkyl nitrate photochemical production rates in North Pacific seawater, *Marine Chemistry*,
566 112, 137-141, <https://doi.org/10.1016/j.marchem.2008.10.002>, 2008.
- 567 Dahl, E. E., Heiss, E. M., & Murawski, K.: The effects of dissolved organic matter on alkyl nitrate production during GOMECC
568 and laboratory studies, *Marine Chemistry*, 142, 11-17, <https://doi.org/10.1016/j.marchem.2012.08.001>, 2012.
- 569 Dahl, E. E., Saltzman, E. S., & de Bruyn, W. J.: The aqueous phase yield of alkyl nitrates from $\text{ROO} + \text{NO}$: Implications for
570 photochemical production in seawater, *Geophysical Research Letters*, 30(6), 1-4,
571 <https://doi.org/10.1029/2002GL016811>, 2003.
- 572 Dahl, E. E., Yvon-Lewis, S. A., & S, S. E.: Saturation anomalies of alkyl nitrates in the tropical Pacific Ocean, *Geophysical*
573 *Research Letters*, 32(L20817), 1-4, <https://doi.org/10.1029/2005GL023896>, 2005.
- 574 Dar, S. S., Ghosh, P., Swaraj, A., & Kumar, A.: Graig-Gordon model validation using observed meteorological parameters
575 and measured stable isotope ratios in water vapor over the Southern Ocean, *Atmospheric Chemistry and Physics*
576 *Discussions*, 20(19), 11435-11449, <https://doi.org/10.5194/acp-20-11435-2020>, 2020.
- 577 Davidson, E. A., & Kingerlee, W.: A global inventory of nitric oxide emissions from soils, *Nutrient Cycling in*
578 *Agroecosystems*, 48, 37-50, 1997.
- 579 Elliot, E. M., Kendall, C., Wankel, S. D., Burns, S. A., Boyer, E. W., Harlin, K., Bain, D. J., & Butler, T. J.: Nitrogen isotopes
580 as indicators of NO_x source contributions to atmospheric nitrate deposition across the Midwestern and Northeastern
581 United States. *Environmental Science and Technology*, 41(22), 7661-7667, <https://doi.org/10.1021/es070898t>, 2007.



- 583 Erbland, J., Vicars, W. C., Savarino, J., Morin, S., Frey, M. M., Frosini, D., Vince, E., Martins, J. M. F.: Air-snow transfer of
584 nitrate on the East Antarctic Plateau - Part 1: Isotopic evidence for a photochemically driven dynamic equilibrium in
585 summer. *Atmospheric Chemistry and Physics*, 13(13), 6403-6419, <https://doi.org/10.5194/acp-13-6403-2013>, 2013.
- 586 Fang, Y. T., Koba, K., Wang, X. M., Wen, D. Z., Li, J., Takebayashi, Y., Liu, X. Y., & Yoh, M.: Anthropogenic imprints on
587 nitrogen and oxygen isotopic composition of precipitation nitrate in a nitrogen-polluted city in southern China.
588 *Atmospheric Chemistry and Physics*, 11, 1313-1325, <https://doi.org/10.5194/acp-11-1313-2011>, 2011.
- 589 Finlayson-Pitts, B. J., & Pitts, J. N.: *Chemistry of the upper and lower troposphere*. San Diego, California: Academic Press,
590 2000.
- 591 Fisher, J. A., Atlas, E. L., Barletta, B., Meinardi, S., Blake, D. R., Thompson, C. R., Ryerson, T. B., Peischl, J., Tzompa-Sosa,
592 Z. A., & Murray, L. T.: Methyl, ethyl and propyl nitrates: global distribution and impacts on reactive nitrogen in
593 remote marine environments, *Journal of Geophysical Research: Atmospheres*, 123(21), 412-429,
594 <https://doi.org/10.1029/2018JD029046>, 2018.
- 595 Frey, M. M., Savarino, J., Morin, S., Erbland, J., & Martins, J. M.: Photolysis imprint in the nitrate stable isotope signal in
596 snow and atmosphere of East Antarctica and implications for reactive nitrogen cycling, *Atmospheric Chemistry and
597 Physics*, 9, 8681-8696, <https://doi.org/10.5194/acp-9-8681-2009>, 2009.
- 598 Freyer, H. D.: Seasonal variation of $^{15}\text{N}/^{14}\text{N}$ ratios in atmospheric nitrate species, *Tellus B: Chemical and Physical Meteorology*
599 , 43(1), 30-44, 1991.
- 600 Freyer, H. D., Kley, D., Volz-Thomas, A., & Kobel, K.: On the interaction of isotopic exchange processes with photochemical
601 reactions in atmospheric oxides of nitrogen, *Journal of Geophysical Research*, 98(D8), 14791-14796, 1993.
- 602 Freyer, H. D., Kobel, K., Delmas, R. J., Kley, D., & Legrand, M. R.: First results of $^{15}\text{N}/^{14}\text{N}$ ratios in nitrate from alpine and
603 polar ice cores, *Tellus B: Chemical and Physical Meteorology*, 48(1), 93-105,
604 <https://doi.org/10.3402/tellusb.v48i1.15671>, 1996.
- 605 Gobel, A. R., Altieri, K. E., Peters, A. J., Hastings, M. G., & Sigman, D. M.: Insights into anthropogenic nitrogen deposition
606 to the North Atlantic investigated using the isotopic composition of aerosol and rainwater nitrate, *Geophysical
607 Research Letters*, 5977-5982, <https://doi.org/10.1002/2013GL058167>, 2013.
- 608 Grannas, A. M., Jones, A. E., Dibb, J., Ammann, M., Anastasio, C., Beine, H. J., Bergin, M., Bottenheim, J., Boxe, C. S.,
609 Carver, G., Chen, G., Crawford, J. H., Domine, F., Frey, M. M., Guzman, M. I., Heard, D. E., Hemig, D., Hoffmann,
610 M. R., Honrath, R. E., Huey, L. G., Hutterli, M., Jacobi, H. W., Klan, P., Lefer, B., McConnell, J., Plane, J., Sander,
611 R., Savarino, J., Shepson, P. B., Simpson, W. R., Sodeau, J. R., von Glasow, R., Weller, R., Wolff, E. W., & Zhu, T.:
612 An overview of snow photochemistry: evidence, mechanisms and impacts, *Atmospheric Chemistry and Physics
613 Discussions*, 7(2), 4165-4283, <https://doi.org/10.5194/acp-7-4329-2007>, 2007.
- 614 Grasshoff, K., Kremling, K., & Ehrhardt, M.: *Methods of seawater analysis*, Verlag Chemie, Florida, 1983.



- 615 Guha, T., Lin, C. T., Bhattacharya, S. K., Mahajan, A. S., Ou-Yang, C.-F., Lan, Y.-P., Hsu, S. C., & Liang, M.-C.: Isotope
616 ratios of nitrate in aerosol samples from Mt. Lulin, a high altitude station in Central Taiwan, *Atmospheric*
617 *Environment*, 154, 53-69, <http://dx.doi.org/10.1016/j.atmosenv.2017.01.036>, 2017
- 618 Guilpart, E., Vimeux, F., Evan, S., Brioude, J., Mertzger, J., Barthe, C., Risi, C., & Cattani, O.: The isotopic composition of
619 near-surface water vapor at the Maito observatory (Reunion Island, southwestern Indian Ocean) documents the
620 controls of the humidity of the subtropical troposphere, *Journal of Geophysical Research: Atmospheres*, 122, 9628-
621 9650, 2017.
- 622 Hamilton, D. S., Lee, L. A., Pringle, K. J., Reddington, C. L., Spracklen, D. V., & Carslaw, K. S.: Occurrence of pristine aerosol
623 environments on a polluted planet, *Proceedings of the National Academy of Sciences*, 111(52), 18466-18471,
624 <https://doi.org/10.1073/pnas.1415440111>, 2014.
- 625 Hastings, M. G., Sigman, D. M., & Lipschultz, F.: Isotopic evidence for source changes of nitrate in rain at Bermuda, *Journal*
626 *of Geophysical Research: Atmospheres*, 108(D24), <https://doi.org/10.1029/2003JD003789>, 2003.
- 627 Haywood, J., & Boucher, O.: Estimates of the direct and indirect radiative forcing due to tropospheric aerosols: a review,
628 *Reviews of Geophysics*, 513-543, 2000.
- 629 Hoering, T.: The isotopic composition of the ammonia and the nitrate ion in rain, *Geochimica et Cosmochimica Acta*, 12(1-
630 2), 97-102, 1957.
- 631 IPCC 2013: Boucher, O. D., Randall, P., Artaxo, C., Bretherton, G., Feingold, P., Forster, V.-M., Kerminen, Y., Kondo, H.,
632 Liao, U., Lohmann, P., Rasch, S.K., Satheesh, S., Sherwood, B., Stevens, & Zhang, X. Y.: Clouds and Aerosols, in:
633 *Climate Change 2013: The Physical Science Basis. Contribution of Working Group I to the Fifth Assessment Report*
634 *of the Intergovernmental Panel on Climate Change*, edited by: Stocker, T.F., Qin, D., Plattner, G.-K., Tignor, M.,
635 Allen, S. K., Boschung, J., Nauels, A., Xia, Y., Bex, V., & Midgley, P. M., Cambridge University Press, Cambridge,
636 United Kingdom and New York, NY, USA, 2013.
- 637 Ishino, S., Hattori, S., Savarino, J., Jourdain, B., Preunkert, S., Legrand, M., Caillon, N., Barbero, A., Kurlbayashi, N., &
638 Yoshida, N.: Seasonal variations of triple oxygen isotopic compositions of atmospheric sulfate, nitrate and ozone at
639 Durmont d'Urville, coastal Antarctica, *Atmospheric Chemistry and Physics*, 17, 3713-3727,
640 <https://doi.org/10.5194/acp-17-3713-2017>, 2017.
- 641 Jacobi, H.-W., & Schrems, O.: Peroxyacetyl nitrate (PAN) distribution over the South Atlantic Ocean, *Physical Chemistry*
642 *Chemical Physics*, 1, 5517-5521, <https://doi.org/10.1039/A905290I>, 1999.
- 643 Jacobi, H.-W., Weller, R., Jones, A. E., Anderson, P. S., & Schrems, O.: Peroxyacetyl nitrate (PAN) concentrations in the
644 Antarctic troposphere measured during the photochemical experiment at Neumayer (PEAN'99). *Atmospheric*
645 *Environment*, 34, 5235-5247, [https://doi.org/10.1016/S1352-2310\(00\)00190-4](https://doi.org/10.1016/S1352-2310(00)00190-4), 2000.
- 646 Jiang, S., Shi, G., Cole-Dai, J., Geng, L., Ferris, D. G., An, C., & Li, Y.: Nitrate preservation in snow at Dome A, East
647 Antarctica from ice core concentration and isotope records, *Atmospheric Environment*, 213, 405-412,
648 <https://doi.org/10.1016/j.atmosenv.2019.06.031>, 2019.



- 649 Johnston, J. C., & Thiemens, M. H. (1997). The isotopic composition of tropospheric ozone in three environments. *Journal of*
650 *Geophysical Research: Atmospheres*, 102(D21), 25395-25404.
- 651 Jones, A. E., Weller, R., Anderson, P. S., Jacobi, H.-W., Wolff, E. W., Schrems, O., & Miller, H.: Measurements of NO_x
652 emissions from the Antarctic snowpack, *Geophysical Research Letters*, 28(8), 1499-1502,
653 <https://doi.org/10.1029/2000GL011956>, 2001.
- 654 Jones, A. E., Weller, R., Minikin, A., Wolff, E. W., Sturges, W. T., McIntyre, H. P., Leonard, S. R., Schrems, O., & Bauguitte,
655 S.: Oxidised nitrogen chemistry and speciation in the Antarctic troposphere, *Journal of Geophysical Research*,
656 104(D17), 21355-21366, <https://doi.org/10.1029/1999JD900362>, 1999.
- 657 Jones, A. E., Weller, R., Wolff, E. W., & Jacobi, H.-W.: Speciation and rate of photochemical NO and NO₂ production in
658 Antarctic snow, *Geophysical Research Letters*, 27(3), 345-348, <https://doi.org/10.1029/1999GL010885>, 2000.
- 659 Kamezaki, K., Hattori, S., Iwamoto, Y., Ishino, S., Furutani, H., Miki, Y., Uematsu, M., Miura, K., & Yoshida, N.: Tracing
660 the sources and formation pathways of atmospheric particulate nitrate over the Pacific Ocean using stable isotopes,
661 *Atmospheric Environment*, 209, 152-166, <https://doi.org/10.1016/j.atmosenv.2019.04.026>, 2019.
- 662 Kendall, C., Elliot, E. M., & Wankel, S. D.: Tracing anthropogenic inputs of nitrogen to ecosystems, in: *Stable isotopes in*
663 *ecology and environmental science*, edited by: Michener, R., & Lajtha, K., Blackwell Publishing, Malden, Mass 375-
664 449, <https://doi.org/10.1002/9780470691854.ch12>, 2007.
- 665 Kim, M. J., Michaud, J. M., Williams, R., Sherwood, B. P., Pomeroy, R., Azam, F., Burkart, M., & Bertram, T. H.: Bacteria-
666 driven production of alkyl nitrates in seawater, *Geophysical Research Letters*, 42, 597-604,
667 <https://doi.org/10.1002/2014GL062865>, 2015.
- 668 Krankowsky, D., Bartecki, F., Klees, G. G., Mauersberger, K., & Schellenbach, K.: Measurement of heavy isotope enrichment
669 in tropospheric ozone, *Geophysical Research Letters*, 22(13), 1713-1716, <https://doi.org/10.1029/95GL01436>, 1995.
- 670 Kroopnick, P., & Craig, H.: Atmospheric oxygen: isotopic composition and solubility fractionation, *Science*, 175(4017), 54-
671 55, 1972.
- 672 Lee, H.-M., Henze, D. K., Alexander, B., & Murray, L. T.: Investigating the sensitivity of surface-level nitrate seasonality in
673 Antarctica to primary sources using a global model, *Atmospheric Environment*, 89, 757-767,
674 <http://dx.doi.org/10.1016/j.atmosenv.2014.03.003>, 2014.
- 675 Michalski, G., Bhattacharya, S. K., & Mase, D. F.: Oxygen isotope dynamics of atmospheric nitrate and its precursor molecules,
676 in: *Handbook of environmental isotope geochemistry. Advances in Isotope Geochemistry*, edited by: Baskaran, M.,
677 Springer, Berlin, Heidelberg, 613-635, https://doi.org/10.1007/978-3-642-10637-8_30, 2012.
- 678 Michalski, G., Scott, Z., Kabling, M., & Thiemens, M. H.: First measurements and modeling of $\Delta^{17}\text{O}$ in atmospheric nitrate,
679 *Geophysical Research Letters*, 30(9), <https://doi.org/10.1029/2003GL017015>, 2003.
- 680 Monks, P. S.: Gas-phase radical chemistry in the troposphere, *Chemical Society Reviews*, 34, 376-395, DOI:
681 10.1039/b307982c, 2005.



- 682 Morin, S., Savarino, J., Frey, M. M., Domine, F., Jacobi, H. W., Kaleschke, L., & Martins, J. M.: Comprehensive isotopic
683 composition of atmospheric nitrate in the Atlantic Ocean boundary layer from 65°S to 79°N, *Journal of Geophysical*
684 *Research*, 114(D05303), 1-19, <https://doi.org/10.1029/2008JD010696>, 2009.
- 685 Nadzir, M. S., Ashfold, M. J., Khan, M. F., Robinson, A. D., Bolas, C., Latif, M. T., Wallis, B. M., Mead, M. I., Hamid, H. H.
686 A., Harris, N. R. P., Ramly, Z. T. A., Lai, G. T., Liew, J. N., Ahamed, F., Uning, R., Samah, A. A., Maulud, K. N.,
687 Suparta, W., Zainudin, S. K., Wahab, M. I. A., Sahani, M., Muller, M., Yeok, F. S., Rahman, N. A., Mujahid, A.,
688 Morris, K. I. & Sasso, N. D.: Spatial-temporal variations in surface ozone over Ushuaia and the Antarctic region:
689 observations from in situ measurements, satellite data, and global models, *Environmental Science and Pollution*
690 *Research*, 25, 2194-2210, <https://doi.org/10.1007/s11356-017-0521-1>, 2018.
- 691 Nesbitt, S. W., Zhang, R., & Orville, R. E.: Seasonal and global NO_x production by lightning estimated from the Optical
692 Transient Detector (OTD), *Tellus B: Chemical and Physical Meteorology*, 52(5), 1206-1215,
693 <https://doi.org/10.3402/tellusb.v52i5.17098>, 2000.
- 694 Park, S. S., & Kim, Y. J.: Source contributions to fine particulate matter in an urban atmosphere, *Chemosphere*, 59, 217-226,
695 <https://doi.org/10.1016/j.chemosphere.2004.11.001>, 2005.
- 696 Park, Y., Park, K., Kim, H., Yu, S., Noh, S., Kim, M.-S., Kim, J.-Y., Ahn, J.-Y., Seok, K.-S., & Kim, Y.-H.: Characterizing
697 isotopic compositions of TC-C, NO₃⁻-N and NH₄⁺-N in PM_{2.5} in South Korea: Impact of China's winter heating,
698 *Environmental Pollution*, 233, 735-744, <https://doi.org/10.1016/j.envpol.2017.10.072>, 2018.
- 699 Rolph, G.D.: Real-time Environmental Applications and Display System (READY) Website (<http://www.ready.noaa.gov>).
700 NOAA Air Resources Laboratory, College Park, MD, 2016.
- 701 Savarino, J., Kaiser, J., Morin, S., Sigman, D. M., & Thiemens, M. H.: Nitrogen and oxygen isotopic constraints on the origin
702 of atmospheric nitrate in coastal Antarctica, *Atmospheric Chemistry and Physics*, 7, 1925-1945,
703 <https://doi.org/10.5194/acp-7-1925-2007>, 2007.
- 704 Schumann, U., & Huntrieser, H.: The global lightning induced nitrogen oxides source, *Atmospheric Chemistry and Physics*
705 *Discussions*, 7(1), 2623-2818, <https://doi.org/10.5194/acp-7-3823-2007>, 2007.
- 706 Shi, G., Buffen, A. M., Hastings, M. G., Li, C., Ma, H., Li, Y., Sun, B., An, C., & Jiang, S.: Investigating the post-depositional
707 processing of nitrate in East Antarctic snow: isotopic constraints in photolytic loss, re-oxidation, and source inputs,
708 *Atmospheric Chemistry and Physics*, 15, 9435-9453, <https://doi.org/10.5194/acp-15-9435-2015>, 2015.
- 709 Shi, G., Buffen, A. M., Ma, H., Hu, Z., Sun, B., Li, C., Yu, J., Ma, T., An, C., Jiang, S., Li, Y., & Hastings, M. G.:
710 Distinguishing summertime atmospheric production of nitrate across the East Antarctic ice sheet, *Geochimica et*
711 *Cosmochimica Acta*, 231, 1-14, <https://doi.org/10.1016/j.gca.2018.03.025>, 2018.
- 712 Shi, G., Ma, H., Zhu, Z., Hu, A., Chen, Z., Jiang, Su., An, C., Yu, J., Ma, T., Li, Y., Sun, B., Hastings, M. G.: Using stable
713 isotopes to distinguish atmospheric nitrate production and its contribution to the surface ocean across hemispheres,
714 *Earth and Planetary Science Letters*, 564, 1-12, <https://doi.org/10.1016/j.epsl.2021.116914>, 2021.



- 715 Sigman, D.M., Casciotti, K.L., Andreani, M., Barford, C., Galanter, M.B.J.K. & Böhlke, J.K.: A bacterial method for the
716 nitrogen isotopic analysis of nitrate in seawater and freshwater, *Analytical chemistry*, 73(17), 4145-4153,
717 <https://doi.org/10.1021/ac010088e>, 2001.
- 718 Spreen, G., Kaleschke, L., & Heygster, G.: Sea ice remote sensing using AMSR-E 89-GHz channels, *Journal of Geophysical*
719 *Research: Oceans*, 113(C02S03), 1-14, <https://doi.org/10.1029/2005JC003384>, 2008.
- 720 Stein, A.F., Draxler, R.R., Rolph, G.D., Stunder, B.J.B., Cohen, M.D., & Ngan, F.: NOAA's HYSPLIT atmospheric transport
721 and dispersion modeling system, *Bull. Amer. Meteor. Soc.*, 96, 2059-2077, [https://doi.org/10.1175/BAMS-D-14-](https://doi.org/10.1175/BAMS-D-14-00110.1)
722 [00110.1](https://doi.org/10.1175/BAMS-D-14-00110.1), 2015.
- 723 Thiemens, M. H.: History and applications of mass-independent isotope effects. *Annual Review of Earth and Planetary*
724 *Sciences*, 34, 217-262, <https://doi.org/10.1146/annurev.earth.34.031405.125026>, 2006.
- 725 van der A, R. J., Eskes, H. J., Boersma, K. F., van Noije, T. P., Van Roozendael, M., De Smedt, I., Peters, D. H. M. U., &
726 Meijer, E. W.: Trends, seasonal variability and dominant NO_x source derived from a ten year record of NO₂ measured
727 from space, *Journal of Geophysical Research*, 113, 1-12, <https://doi.org/10.1029/2007JD009021>, 2008.
- 728 Vicars, W. C., Savarino, J.: Quantitative constraints on the ¹⁷O-excess ($\Delta^{17}\text{O}$) signature of surface ozone: Ambient
729 measurements from 50°N to 50°S using the nitrite-coated filter technique. *Geochimica et Cosmochimica Acta*, 135,
730 270-287, <https://doi.org/10.1016/j.gca.2014.03.023>, 2014.
- 731 Virkkula, A., Teinila, K., Hillamo, R., Kerminen, V. M., Saarikoski, S., Aurela, M., Viidanoja, J., Paatero, J., Koponen, I. K.,
732 & Kulmala, M.: Chemical composition of boundary layer aerosol over the Atlantic Ocean and at an Antarctic site,
733 *Atmospheric Chemistry and Physics*, 6(11), 3407-3421, <https://doi.org/10.5194/acp-6-3407-2006>, 2006.
- 734 Walters, W. W., & Michalski, G.: Theoretical calculation of nitrogen isotope equilibrium exchange fractionation factors for
735 various NO_y molecules, *Geochimica et Cosmochimica Acta*, 164, 284-297,
736 <http://dx.doi.org/10.1016/j.gca.2015.05.029>, 2015.
- 737 Walters, W. W., & Michalski, G.: Theoretical calculation of oxygen equilibrium isotope fractionation factors involving various
738 NO_y molecules, OH, and H₂O and its implications for isotope variations in atmospheric nitrate, *Geochimica et*
739 *Cosmochimica Acta*, 191, 89-101, <http://dx.doi.org/10.1016/j.gca.2016.06.039>, 2016.
- 740 Walters, W. W., Michalski, G., Böhlke, J. K., Alexander, B., Savarino, J., & Thiemens, M. H.: Assessing the seasonal dynamics
741 of nitrate and sulfate aerosols at the South Pole utilizing stable isotopes, *Journal of Geophysical Research:*
742 *Atmospheres*, 124(14), 8161-8177, <https://doi.org/10.1029/2019JD030517>, 2019.
- 743 Walters, W. W., Simonini, D. S., & Michalski, G.: Nitrogen isotope exchange between NO and NO₂ and its implications for
744 $\delta^{15}\text{N}$ variations in tropospheric NO_x and atmospheric nitrate, *Geophysical Research Letters*, 43, 440-448,
745 <https://doi.org/10.1002/2015GL066438>, 2016.
- 746 Weller, R., Jones, A. E., Wille, A., Jacobi, H.-W., McIntyre, H. P., Sturges, W. T., Huke, M., & Wagenback, D.: Seasonality
747 of reactive nitrogen oxides (NO_y) at Neumayer Station, Antarctica, *Journal of Geophysical Research*, 107(D23), 1-
748 11, <https://doi.org/10.1029/2002JD002495>, 2002.



- 749 Williams, J. E., Le Bras, G., Kukui, A., Ziereis, H., Brenninkmeijer, C. A. M.: The impact of the chemical production of methyl
750 nitrate from the $\text{NO} + \text{CH}_3\text{O}_2$ reaction on the global distributions of alkyl nitrates, nitrogen oxides and tropospheric
751 ozone: a global modelling study. *Atmospheric Chemistry and Physics*, 14(5), 2363-2382, [https://doi.org/10.5194/acp-](https://doi.org/10.5194/acp-14-2363-2014)
752 14-2363-2014, 2014.
- 753 Yeatman, S. G., Spokes, P. F., Dennis, P. F., & Jickells, T. D.: Comparisons of aerosol nitrogen isotopic composition at two
754 polluted coastal sites, *Atmospheric Environment*, 35, 1307-1320, [https://doi.org/10.1016/S1352-2310\(00\)00408-8](https://doi.org/10.1016/S1352-2310(00)00408-8),
755 2001.
- 756 Zong, Z., Wang, X., Tian, C., Chen, Y., Fang, Y., Zhang, F., Li, C., Sun, J., Li, J., & Zhang, G.: First assessment of NO_x
757 sources at a regional background site in North China using isotopic analysis linked with modeling, *Environmental*
758 *Science and Technology*, 51, 5923-5931, <https://doi.org/10.1021/acs.est.6b06316>, 2017.
- 759